JOURNAL OF AGRICULTURAL AND FOOD CHEMISTRY

pubs.acs.org/JAFC Article

Synthesis and Photoactivated Toxicity of 2-Thiophenylfuranocoumarin Induce Midgut Damage and Apoptosis in *Aedes aegypti* Larvae

Jiecheng Wu,[§] Lanying Wang,[§] Yunfei Zhang, Shujing Zhang, Shakil Ahmad, and Yanping Luo*

Cite This: *J. Agric. Food Chem.* 2021, 69, 1091−1106

Read Online

ACCESS | Metrics & More | Article Recommendations

ABSTRACT: Furanocoumarins are photoactive compounds derived from secondary plant metabolites. They possess many bioactivities, including antioxidative, anticancer, insecticidal, and bactericidal activities. Here, we designed a new scheme for synthesizing 2-arylfuranocoumarin derivatives by condensation, esterification, bromination, and Wittig reaction. We found that 2-thiophenylfuranocoumarin (Iy) had excellent photosensitive activity. Three Iy concentrations (LC_{25}, LC_{50}, and LC_{75}) were used to treat the fourth instar larvae of *Aedes aegypti* (*A. aegypti*). The photoactivated toxicity, sublethal dose, mitochondrial dysfunction, oxidative stress level, intestinal barrier dysfunction, and apoptosis were studied. The results showed that Iy induced reactive oxygen species (ROS) production in midgut cells under ultraviolet light. Ultrastructural analysis demonstrated that mitochondria were damaged, and the activities of related enzymes were inhibited. Ultimately, Iy exposure led to excessive ROS production followed by the inhibition of antioxidant enzymes, including SOD, CAT, GPx, and GR, which diminished ROS elimination and escalated oxidative stress in midgut cells, aggravating the degree of oxidative damage in these cells. Histopathological changes were observed in the midgut, which led to intestinal barrier dysfunction. When the elimination of ROS was blocked and it accumulated in cells, apoptosis-related genes, including *AeDronc*, *AeCaspase7*, and *AeCaspase8*, were induced and activated. In addition, Iy affected the growth and development of *A. aegypti* at sublethal concentrations, and there was an obvious post-lethal effect. Thus, we found that Iy caused midgut damage and apoptosis in *A. aegypti* larvae under ultraviolet light, which preliminarily revealed the mode of action of Iy in *A. aegypti*.

KEYWORDS: *2-thiophenylfuranocoumarin, Aedes aegypti, midgut, oxidative stress, apoptosis*

1. INTRODUCTION

Furanocoumarins are photosensitive compounds produced as secondary metabolites by plants to resist the attack of fungi, bacteria, and insects.[1−3] In humans, furanocoumarins have broad application prospects as anti-inflammatory and anti-oxidative agents, along with their therapeutic potential in the treatment of skin diseases and cancer.[4−6] Due to their antibacterial and insecticidal properties, furanocoumarins are regarded as natural pesticides.[7] Irradiation of furanocoumarins by ultraviolet light causes electron transition and change to the triplet state. The triplet status is persistent *in vivo* and involved in energy transfer and phototoxicity.[8,9] Furanocoumarins can produce reactive oxygen species (ROS) and damage cells through lipid peroxidation, enzyme inactivation, guanine oxidation, and nucleic acid fragmentation.[3,10−12] In eukaryotic cells, mitochondria are critically involved in metabolite biosynthesis and the production of the energy carrier molecule ATP.[13] Typically, ROS originates from the electron transport chain (ETC).[14] Specifically, nicotinamide adenine dinucleotide (NADH) and reduced flavin adenine dinucleotide ($FADH_2$) produced by the tricarboxylic acid (TCA) cycle provide electrons to the ETC complexes I and II, respectively.[15] When the mitochondria are damaged, ETC electrons leak, and ROS are produced in the form of superoxide anions.[16] Excessive ROS levels can lead to oxidative stress.[17,18] Among biological antioxidant defense systems, superoxide dismutase (SOD) is the first line of defense.[19] SOD converts O_2^- into hydrogen peroxide (H_2O_2), which is decomposed into water by the catalase (CAT) reaction. Concurrently, glutathione peroxidase (GPx) catalyzes the reaction of glutathione (GSH) with H_2O_2 to form water,[20] which reduces the ROS level *in vivo*. Glutathione reductase (GR) can reduce oxidized glutathione (GSSG) to GSH, which regenerates the antioxidant capacity of the GSH antioxidant system. The ratio of GSH to GSSG reflects the redox state of the organism,[21] while the levels of malondialdehyde (MDA) and protein carbonyl reflect the degree of lipid peroxidation and protein oxidation, respectively.[22,23]

Aedes aegypti (*A. aegypti*) is an effective vector of dengue fever, yellow fever, chikungunya fever, and other important viral diseases. It is a global problem endangering public health.[24−26] Photosensitizers with insecticidal activity are

Received: November 16, 2020
Revised: December 31, 2020
Accepted: December 31, 2020
Published: January 12, 2021

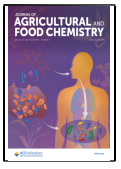

https://dx.doi.org/10.1021/acs.jafc.0c07237
J. Agric. Food Chem. 2021, 69, 1091−1106

environmentally friendly and have a broad application prospect in mosquito control.[27] In *A. aegypti*, the core apoptosis pathway depends on the initiator caspase AeDronc. Upon induction by an apoptotic signal, the initiator caspase AeDronc binds to its adaptor molecule AeArk and activates the downstream caspases AeCaspase7 and AeCaspase8, leading to apoptosis.[28,29] This process is blocked by the *A. aegypti* inhibitor of apoptosis protein 1 (AeIAP1), which inhibits apoptosis through direct interaction with AeDronc, AeCaspase7, and AeCaspase8. AeMichelob_x is an antagonist molecule of AeIAP1 that can neutralize the inhibitory effect of AeIAP1 on caspases and promote apoptosis.[30]

In this study, we designed a new scheme for synthesizing 2-arylfuranocoumarin derivatives from resorcinol by condensation, esterification, bromination, and Wittig reaction. We assessed the fluorescence properties of the newly synthesized derivatives. An *in vivo* assessment of target compound 2-thiophenylfuranocoumarin (Iy) found that it exerted excellent photoactivated toxicity in *A. aegypti* larvae. Therefore, the effects of Iy on the growth and development of *A. aegypti* larvae at sublethal concentrations were evaluated. Furthermore, the mechanism of midgut damage was elucidated by measuring the oxidative stress level, performing a histological and ultrastructural analysis of midgut paraffin sections using a transmission electron microscope, and assessing the permeability of the peritrophic membrane. Finally, a series of physiological conditions related to apoptosis were applied to study cell apoptosis.

2. MATERIALS AND METHODS

2.1. Test Materials and Equipment. The susceptible strain of *A. aegypti* was provided by the Agricultural and Pharmaceutical Laboratory at Hainan University, Haikou, China. *A. aegypti* was reared, as described previously.[31]

The ROS assay kit, mitochondrial membrane potential (MMP) assay kit, and oxidative stress and mitochondria-related indicator assay kit were purchased from Solarbio Technology Company (Solarbio, Beijing, China). The protein concentration assay kit and apoptosis staining kit were purchased from Beyotime Biotechnology Company (Beyotime Biotechnology, Shanghai, China). All other commercially available chemical reagents were analytically pure or chemically pure.

Equipment included the micro melting point apparatus (Yanagimoto, Kyoto, Japan), an AV 400 NMR spectrometer (Bruker, Watertown, MA, USA; $CDCl_3$ was used as a solvent), a Trace MS 2000 GS-MS (Thermo Finnigan, San Jose, CA, USA), a Vario EL III element analyzer (Elementar, Langenselbold, Germany), and a mixer mill MM400 frozen (Retsch, Haan, Germany).

2.2. Synthesis of Furan [3,2-g] Coumarin I. *2.2.1. Synthesis of 7-Hydroxy-4,6-dimethylcoumarin 2.* In a 250 mL round-bottom flask, 12.4 g (0.1 mol) of 4-methyl-1,3-resorcinol and 50 mL of concentrated sulfuric acid were mixed in an ice bath for 1 h, during which 0.12 mol of ethyl acetoacetate (or ethyl 2-chloroacetoacetate) was added by slowly dripping into the mixture. Then, the ice bath was removed, and the solution was stirred overnight at 25 °C. The resulting reaction solution was poured into an ice-water mixture. A large amount of a light-yellow precipitate formed, which was recovered as white solid 2 by vacuum filtration.

2.2.2. Synthesis of 7-Ester-4,6-dimethylcoumarin 3. One mmol of 7-hydroxy-4,6-dimethylcoumarin 2 and 0.17 g of anhydrous K_2CO_3 were placed in a grinding container, and 1.1 mmol of substituted aryl chloride was quickly added. The mix was ground for 15 min at 30 Hz. Then, the reaction mix was checked by thin-layer chromatography (TLC), washed, and filtered. The product, 7-ester-4,6-dimethylcoumarin 3, was obtained by recrystallization with anhydrous ethanol.

2.2.3. Synthesis of Target Compound I. In a 25 mL round-bottom flask, 1.0 mmol of 7-ester coumarin 3 and 1.1 mmol of *N*-bromosuccinimide (NBS) were mixed with a catalytic amount of benzoyl peroxide and 10 mL of anhydrous benzene then heated and refluxed. The reaction was monitored by TLC for approximately 6−10 h. The resulting reaction mixture was concentrated into a solid under reduced pressure, washed with hot water, filtered, and dried. The product was recrystallized with glacial acetic acid to obtain 6-bromomethyl-7-ester coumarin 4, which was used in the next step without further purification.

Using a 25 mL round-bottom flask, 6-bromomethyl-7-ester coumarin 4 (1.0 mmol), triphenylphosphine (1.0 mmol), and 10 mL of anhydrous CH_3Cl were mixed. The reaction was monitored by TLC after heating and refluxing. The reaction mixture was concentrated until a solid was formed, which was washed with toluene and filtered to obtain 6-bromotriphenylphosphine methyl-7-ester coumarin 5. Without further purification, the resulting material was used in the next step.

The six-fold amount of anhydrous K_2CO_3 and 10 mL of anhydrous tetrahydrofuran (THF) were added to the product described above. The reaction, which was performed under stirring at room temperature for approximately 4−10 h, was monitored by TLC. The products were separated by silica gel (200−300 mesh) column chromatography using petroleum ether-ethyl acetate (10/1, v/v) as a mobile phase. White or yellow solid I was produced.

2.2.4. Test Method for Insecticidal Activity of Target Compound I. In the study on the activity of target compound I, compound I was dissolved in acetone and prepared into a solution of 100 mg/L with dechlorinated water, and the mosquito species tested was *Culex pipiens pallens*. The fourth instar larvae of *Culex pipiens pallens* were exposed to 100 mg/L compound I solution for 3 h in the dark. Then, the larvae were exposed under a 365 nm black light lamp (Hitachi 6 W, 17 cm away from the culture dish) for 3 h and placed again in the dark for 42 h. Finally, the mortality of larvae was calculated.

2.3. Toxicity Test. Thirty *A. aegypti* larvae at the fourth instar were randomly selected and placed into culture dishes containing 9.8 mL of dechlorinated water, to which six different concentrations (2000, 2500, 3000, 3500, 4000, and 4500 mg/L) of 0.2 mL of Iy solution were added. Therefore, the final concentration of the solution was 40, 50, 60, 70, 80, and 90 mg/L, respectively. The fourth instar larvae were placed in the dark for 3 h to fully absorb the solution. Then, the larvae were exposed under a 365 nm black light lamp (Hitachi 6 W, 17 cm away from the culture dish) for 3 h and placed again in the dark for 42 h. The solvent control was created by adding 0.2 mL of acetone to 9.8 mL of dechlorinated water, and the blank control consisted of 10 mL of dechlorinated water. Five replicates of each concentration were used, and each experiment was repeated three times. The mortality and toxicity caused by Iy were measured by enumerating dead and surviving larvae.

2.4. Effect of Sublethal Dose on Larval Development Parameters. Based on the calculated toxicity of Iy, the larvae were treated at different sublethal concentrations, and the effects of Iy on larval growth and development were evaluated, along with the post-lethal effect. Three hundred fourth instar larvae were randomly selected and exposed to LC_{10}, LC_{20}, and LC_{30} (45, 51, and 56 mg/L) of Iy solution, using the same procedure as in the toxicity test. The larval death numbers of the treatment and control groups were examined after 48 h, and the larval mortality was calculated.

The surviving larvae were washed 3 times with dechlorinated water and raised normally. The pupae were collected and placed in adult cages. The numbers of pupae and eclosion mosquitoes were regularly checked every day. The cumulative pupation rate and emergence rate were calculated, and the average pupation time and average emergence time were documented. Furthermore, the numbers of dead pupae and abnormal eclosion mosquitoes were regularly recorded every day. The collected data were used to calculate the dead pupa rate (dead pupa number/total pupa number) and the abnormal emergence rate (abnormal eclosion mosquito number/total eclosion mosquito number).

2.5. Detection of Singlet Oxygen ($^1O_2$). The previously published method for measuring $^1O_2$ was slightly modified in the present study.[32] Samples containing 100 mg/L Iy and 10×10^{-3} mol/

https://dx.doi.org/10.1021/acs.jafc.0c07237
J. Agric. Food Chem. 2021, 69, 1091−1106

L 2,2,6,6-tetramethylpiperidine (Macklin, Shanghai, China) were irradiated with 365 nm black light for 30 min. The $^1O_2$ production was detected by electron spin resonance (ESR) spectroscopy using the AV 400 NMR spectrometer (Bruker). The ESR parameter settings for measuring $^1O_2$ in this experiment were as follows: center field, 3565G; power, 20.02 mW; modulation frequency, 100 kHz; time constant, 2.56 ms; receiver gain, 1×10^3).

2.6. Detection of ROS. We used a previously described ROS detection method with some modifications.[33] The larvae were treated with 65 mg/L Iy. The whole digestive organ system was recovered by dissection at 0, 1, 2, 3, and 4 h after light treatment followed by incubation in 2 μmol/L 2,7-dichloro-hydrofluorescein diacetate (DCFH-DA) for 30 min. ROS production was analyzed qualitatively and quantitatively. To perform a qualitative analysis, samples loaded with the probe were washed three times with phosphate-buffered saline (PBS), and green fluorescence signals were observed with an Olympus BX53 fluorescence microscope (Olympus Corporation, Tokyo, Japan) using 488 and 525 nm for excitation and emission, respectively. For quantitative analysis, 30 digestive organs were submerged in 5 mL of ultrapure water and completely ground with a glass bead homogenizer. The tissue homogenates were centrifuged at 11,000g for 10 min at 4 °C, and the supernatants were collected for fluorescence measurements with a multifunction enzyme labeling instrument (PerkinElmer, Waltham, MA, USA) using 488 and 525 nm for excitation and emission, respectively. The results were expressed as fold changes in fluorescence intensity at 1 h intervals over the value measured at 0 h.

2.7. Observation by Transmission Electron Microscopy (TEM). The dissected midgut was cleaned with PBS and fixed overnight in 2.5% glutaraldehyde solution. The samples were processed as previously described and analyzed using a TEM instrument (Hitachi, Tokyo, Japan).[34]

2.8. Detection of Mitochondrial and Oxidative Stress Indicators. The 60 midguts were dissected, washed with PBS, and weighed before being ground with a glass bead homogenizer. The tissue homogenates were used to detect mitochondria and oxidative stress indicators. The protein concentrations of the samples were normalized based on the results obtained with the Bradford protein concentration assay kit (Solarbio).

The indicators of oxidative stress, including SOD, CAT, GR, GPx, GSH, GSSG, MDA, and protein carbon, were determined by a kit (cat. nos. BC0175, BC0200, BC1165, BC1190, BC1175, BC1185, BC0025, and BC1270, Solarbio). Mitochondria-related indicators, including complex I, complex II, complex III, complex IV, citric acid synthase (CS), isocitrate dehydrogenase (ICDHm), α-ketoglutarate dehydrogenase (α-KGDH), and ATP, were evaluated according to the manufacturer's instructions. (cat. nos. BC0515, BC3235, BC3245, BC0945, BC1065, BC2165, BC0715, and BC0305, Solarbio).

2.9. Detection of Mitochondrial Membrane Potential (MMP). As previously described,[35] the dissected midgut samples were incubated with 5,5,6,6-tetrachloro-1,1,3,3-tetraethylbenzimidazolyl carbocyanine iodide (JC-1) staining solution for 20 min at 37 °C then washed three times with JC-1 staining buffer. Green fluorescence of JC-1 monomers was detected at 490/530 nm (excitation/emission), and red fluorescence of JC-1 aggregates was observed at 525/590 nm (excitation/emission). The images were captured with the Olympus BX53 fluorescence microscope. ImageJ software was used to choose the images with the same exposure time for statistical analysis of MMP, and the ratio of green to red fluorescence was calculated. Each calculation was based on ten images selected for the statistical analysis.

2.10. Histopathological Evaluation of the Midgut. Iy-treated larvae were fixed in 4% paraformaldehyde solution for 48 h. The samples were processed as described previously,[36] observed under a light microscope (Carl Zeiss AG, Oberkochen, Germany), and the pictures were taken.

2.11. Detection of Peritrophic Membrane Permeability. As previously described,[37] the surviving larvae were washed three times with chlorinated water and submerged in 0.5 mg/mL fluorescein isothiocyanate (FITC)-dextran, 40 kDa (Sigma-Aldrich, St. Louis, MO, USA), for 1 h (unbound FITC was removed by a Sephadex gel G10 column). The stained larvae were washed three times with dechlorinated water and placed in an ice bath for 10 min to slow down their activity for microscopic analysis using the SZX16 fluorescence microscope (Olympus). Green fluorescence of FITC in the larvae was measured using the GFP channel, and spontaneous fluorescence was captured using the RFP channel for subsequent colocation analysis.

2.12. Detection of Chitin Content. Thirty midguts were dissected and washed with PBS before determining the wet weight. The midgut samples were ground in 1 mL of ultrapure water using a glass bead homogenizer. The samples were processed, as described previously.[38] The absorbance was measured at 650 nm using an ultraviolet−visible spectrophotometer (MAPADA, Shanghai, China). A stock solution containing 100 mg/L glucosamine (Sigma-Aldrich) was used to construct a standard curve for normalizing the chitin content values, which were expressed based on the amount of glucosamine.

2.13. Terminal Deoxynucleotidyl Transferase dUTP Nick End Labeling (TUNEL) Assay. TUNEL staining was performed as previously described, with some modifications.[39] The one-step TUNEL cell apoptosis assay kit was used to assess the apoptosis status. The midgut samples were incubated in 100 μL of TUNEL solution at 37 °C for 1 h and then washed three times with PBS. Apoptosis was observed using the Olympus BX53 fluorescence microscope. Appropriate filters were selected for the excitation wavelength range of 450−500 nm and the emission wavelength range of 515−565 nm.

2.14. Hoechst 33342 Staining. According to the manufacturer's instructions, the midgut samples were incubated in 1 mL of Hoechst 33342 working solution at 4 °C for 30 min followed by three times washing with PBS. Apoptosis was observed using the Olympus BX53 fluorescence microscope at 350/461 nm (excitation/emission).

2.15. Quantitative Reverse Transcription PCR (RT-qPCR). For the RT-qPCR analysis, we used primer sequences as published previously.[31] Total RNA was extracted from 15 midgut samples with the TRIzol RNA reagent kit (Thermo Scientific, Waltham, MA, USA), and the first-strand cDNA was synthesized using the RevertAid First Strand cDNA Synthesis Kit (Thermo Scientific). The qPCR step was performed using the SYBR Select Master Mix (2X) kit (ABI, Waltham, MA, USA) with a total volume of 20 μL. The amplification conditions were as follows: predenaturation at 95 °C for 10 min was followed by 40 cycles of 95 °C for 15 s and 60 °C for 60 s. Dissolution curve analysis was performed as follows: at 95 °C for 15 s, at 60 °C for 60 s, and at 95 °C for 15 s. The expression levels of *AeDronc*, *AeCaspase7*, *AeCaspase8*, *AeIAP1*, *AeMichelob_x*, and the housekeeping gene *RP7S* were analyzed. Using the *RP7S* gene as the reference gene, the relative gene expression was calculated by the $2^{-\Delta\Delta Ct}$ method.

2.16. Statistical Analysis. All experiments were carried out in triplicate and repeated three times, at least. Representative data values are expressed as the mean ± standard deviation (SD). The analysis of variance and Duncan's test (SPSS 23.0) were used to evaluate the difference between the average values of each treatment. The results were considered statistically significant when the probability (p) value was <0.05.

3. RESULTS

3.1. Chemistry. Coumarin 2 was synthesized from *O*-methylresorcinol and 1-dicarbonyl compound 1 in the presence of concentrated sulfuric acid, and ester compound 3 was obtained by the reaction of aryl chloride with compound 2 in the presence of triethylamine; the physicochemical properties of compound 3 derivatives are shown in Table 1. Compound 4 was brominated by NBS at the methyl group on position 6 of the coumarin core. Resulting compound 4 was reacted with triphenylphosphine (PPh_3) to form Wittig reagent 5. In the presence of K_2CO_3, compound 5 underwent an

https://dx.doi.org/10.1021/acs.jafc.0c07237
J. Agric. Food Chem. 2021, 69, 1091−1106

Table 1. Physicochemical Properties of Compound 3 Derivatives

no.	R^1	R^2	yield (%)	m. p. (°C)	physical state
3a	C_6H_5	H	100	179–181	white crystal
3b	2-F-C_6H_4	H	97	219–221	white crystal
3c	3-F-C_6H_4	H	95	210–212	white crystal
3e	2-F-C_6H_4	Cl	90	213–214	white crystal
3f	3-F-C_6H_4	Cl	93	221–222	white solid
3g	4-F-C_6H_4	Cl	91	185–187	white crystal
3i	3-Cl-C_6H_4	H	96	223–225	white solid
3j	4-Cl-C_6H_4	H	100	202–204	white crystal
3m	3,4-2F-C_6H_3	H	92	233–234	white solid
3p	2,4-2Cl-C_6H_3	H	94	240–242	white crystal
3t	3-CF_3-C_6H_3	H	95	206–207	white crystal
3u	4-CF_3-C_6H_3	H	94	188–189	white crystal
3w	4-OCH_3-C_6H_4	H	96	222–224	white crystal
3x	C_4H_3O	H	90	191–192	white crystal
3y	C_4H_3S	H	87	222–224	white crystal
3aa	1-$C_{10}H_7$	H	96	216–218	white crystal
3bb	2-$C_{10}H_7$	H	94	235–237	white crystal
3cc	C_3H_5	H	85	128–130	white crystal

Table 2. Physicochemical Properties of Target Compound I Derivatives

no.	R^1	R^2	yield (%)	m. p. (°C)	physical state
Ia	C_6H_5	H	89	216–218	white solid
Ib	2-F-C_6H_4	H	84	227–229	white solid
Ic	3-F-C_6H_4	H	86	249–250	yellow solid
Ie	2-F-C_6H_4	Cl	80	257–259	white solid
If	3-F-C_6H_4	Cl	83	260–262	white solid
Ig	4-F-C_6H_4	Cl	74	254–256	white solid
Ii	3-Cl-C_6H_4	H	90	239–241	white solid
Ij	4-Cl-C_6H_4	H	88	216–218	white solid
Im	3,4-2F-C_6H_3	H	76	218–220	white solid
Ip	2,4-2Cl-C_6H_3	H	88	228–230	white solid
It	3-CF_3-C_6H_3	H	69	208–210	white solid
Iu	4-CF_3-C_6H_3	H	75	215–217	white solid
Iw	4-OCH_3-C_6H_4	H	87	204–206	yellow solid
Ix	C_4H_3O	H	69	187–189	white solid
Iy	C_4H_3S	H	74	190–192	white solid
Iaa	1-$C_{10}H_7$	H	84	235–237	white solid
Ibb	2-$C_{10}H_7$	H	89	246–248	white solid
Icc	C_3H_5	H	79	123–125	white solid

intramolecular Wittig reaction to generate target compound I (Scheme 1); the physicochemical properties of target compound I derivatives are shown in Table 2.

The synthesis of the target compound requires bromination, along with Wittig reagent preparation and reaction, which depend on humidity-sensitive substances. To minimize the effect of environmental humidity and other factors, our newly designed synthesis scheme combined the three synthesis steps without purifying the intermediates, which were directly used as substrates in the next reaction to obtain target compound I.

3.1.1. Spectral Analysis of Coumarin 2. 7-Hydroxy-4,6-dimethylcoumarin (2a): The yield is 96%, m. p. 258–260 °C (literature value 268 °C). ^{1}H NMR (400 MHz, $CDCl_3$): δ 7.33 (s, 1H), 6.87 (s, 1H), 6.13 (s, 1H), 6.03 (s, 1H), 2.40 (s, 3H), 2.31 (s, 3H).

3-Chloro-7-hydroxy-4,6-dimethylcoumarin (2b): The yield is 83%, m. p. 242–244 °C. ^{1}H NMR (400 MHz, $CDCl_3$): δ 7.14 (s, 1H), 6.98 (s, 1H), 5.12 (s, 1H), 2.53 (s, 3H), 2.35 (s, 3H).

3.1.2. Spectral Analysis of Compound 3. Nuclear magnetic resonance (NMR) results show that there was a single peak near 6.28 ppm for the 3-position hydrogen of the coumarins. If the 3-position hydrogen was replaced by chlorine, this peak will disappear. There was a single peak between 2.4 and 2.6 ppm for the 4-methyl group. If there was chlorine substitution in the adjacent position, the chemical shift will move to the high field. There was a single peak near 2.32 ppm for the chemical shift of 6-methyl. The mass spectra showed that the molecular ion peaks were unstable and the abundance was low.

3.1.2.1. 4,6-Dimethyl-2-oxo-2H-chromen-7-yl-benzoate (3a). ^{1}H NMR (400 MHz, $CDCl_3$): δ 8.30–8.13 (m, 2H), 7.68 (dd, J = 10.6, 4.4 Hz, 1H), 7.54 (dd, J = 18.5, 11.0 Hz, 3H), 7.20 (s, 1H), 6.28 (s, 1H), 2.45 (s, 3H), 2.31 (s, 3H). MS (EI): m/z (%) 294 ([M]$^+$, 4.58), 105 (100), 77 (41.08). Anal. calcd for $C_{18}H_{14}O_4$: C, 73.46; H, 4.79. Found: C, 73.48; H, 4.81.

3.1.2.2. 4,6-Dimethyl-2-oxo-2H-chromen-7-yl-2-fluoro-benzoate (3b). ^{1}H NMR (400 MHz, $CDCl_3$): δ 8.13 (t, J = 7.6, 1H), 7.73–7.56 (m, 1H), 7.50 (s, 1H), 7.31 (t, J = 7.6 Hz, 1H), 7.28–7.23 (m, 1H), 7.21 (s, 1H), 6.27 (s, 1H), 2.45 (s, 3H), 2.33 (s, 3H). ^{13}C NMR (100 MHz, $CDCl_3$): δ 163.31, 162.01, 160.67, 152.43, 151.76, 135.74, 132.69, 126.94, 126.40, 124.37, 124.33, 118.18, 117.49, 117.27, 114.78, 110.94, 77.34, 77.18, 77.02, 76.82, 76.70, 18.73, 16.18. MS (EI): m/z (%)

Scheme 1. Synthesis of 2-Substituted Aryl-7*H*-furo [3,2-*g*] Coumarin I. (a) H_2SO_4 and Ice; (b) ArCOCl and K_2CO_3; (c) NBS, Benzene, and Reflux; (d) PPh_3, $CHCl_3$, and Reflux; (e) K_2CO_3 and THF. R^1 = H and Cl. Ar = Aryl Substitution.

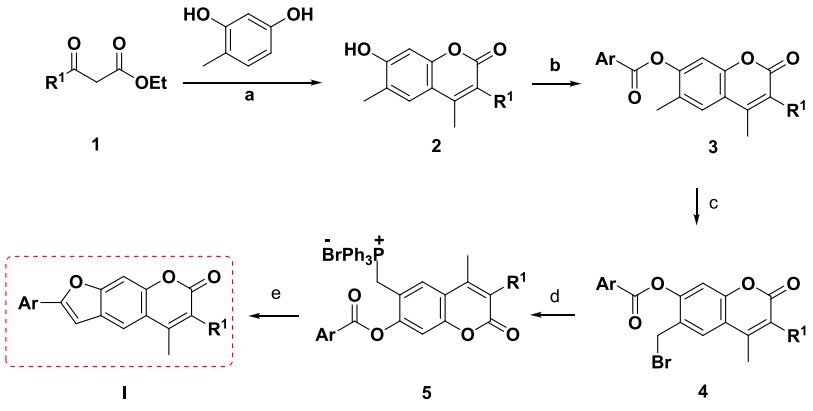

https://dx.doi.org/10.1021/acs.jafc.0c07237
J. Agric. Food Chem. 2021, 69, 1091–1106

312 ([M]$^+$, 7), 161 (1), 123 (100), 95 (17), 75 (3). Anal. calcd for $C_{18}H_{13}FO_4$: C, 69.23; H, 4.20. Found: C, 69.22; H, 4.23.

3.1.2.3. 4,6-Dimethyl-2-oxo-2H-chromen-7-yl-3-fluorobenzoate (3c). ^{1}H NMR (400 MHz, $CDCl_3$): δ 8.02 (d, J = 7.8 Hz, 1H), 7.96−7.85 (m, 1H), 7.61−7.45 (m, 2H), 7.39 (dd, J = 8.3, 2.6 Hz, 1H), 7.19 (s, 1H), 6.28 (s, 1H), 2.45 (s, 3H), 2.30 (s, 3H). MS (EI): m/z (%) 312 ([M]$^+$, 9), 161 (1), 123 (100), 95 (28). Anal. calcd for $C_{18}H_{13}FO_4$: C, 69.23; H, 4.20. Found: C, 69.25; H, 4.24.

3.1.2.4. 3-Chloro-4,6-dimethyl-2-oxo-2H-chromen-7-yl-2-fluorobenzoate (3e). ^{1}H NMR (400 MHz, $CDCl_3$): δ 8.13 (m, J = 7.6, 1.8 Hz, 1H), 7.78−7.61 (m, 1H), 7.53 (s, 1H), 7.36−7.26 (m, 2H), 2.60 (s, 3H), 2.35 (s, 3H). MS (EI): m/z (%) 346 ([M]$^+$, 4), 123 (100), 95 (15), 75 (2). Anal. calcd for $C_{18}H_{12}ClFO_4$: C, 62.35; H, 3.49. Found: C, 62.38; H, 3.46.

3.1.2.5. 3-Chloro-4,6-dimethyl-2-oxo-2H-chromen-7-yl-3-fluorobenzoate (3f). ^{1}H NMR (400 MHz, $CDCl_3$): δ 8.02 (d, J = 7.8 Hz, 1H), 7.90 (d, J = 8.9 Hz, 1H), 7.54 (d, J = 5.2 Hz, 2H), 7.39 (d, J = 2.4 Hz, 1H), 7.23 (s, 1H), 2.61 (s, 3H), 2.32 (s, 3H). MS (EI): m/z (%) 346 ([M]$^+$, 7), 139 (5), 123 (100), 95 (27), 75 (4). Anal. calcd for $C_{18}H_{12}ClFO_4$: C, 62.35; H, 3.49. Found: C, 62.36; H, 3.50.

3.1.2.6. 3-Chloro-4,6-dimethyl-2-oxo-2H-chromen-7-yl-4-fluorobenzoate (3g). ^{1}H NMR (400 MHz, $CDCl_3$): δ 8.25 (dd, J = 8.9, 5.4 Hz, 2H), 7.27 (s, 1H), 7.22 (dd, J = 9.9, 7.3 Hz, 3H), 2.61 (s, 3H), 2.32 (s, 3H). MS (EI): m/z (%) 346 ([M]$^+$, 5), 123 (100), 95 (22), 75 (3). Anal. calcd for $C_{18}H_{12}ClFO_4$: C, 62.35; H, 3.49. Found: C, 62.36; H, 3.44.

3.1.2.7. 4,6-Dimethyl-2-oxo-2H-chromen-7-yl-3-chlorobenzoate (3i). ^{1}H NMR (400 MHz, $CDCl_3$): δ 8.08 (d, J = 8.4 Hz, 2H), 7.85−7.62 (m, 2H), 7.49 (s, 1H), 7.18 (s, 1H), 6.28 (s, 1H), 2.45 (s, 3H), 2.29 (s, 3H). MS (EI): m/z (%) 374 ([M]$^+$, 7), 183 (100), 157 (15), 104 (3), 76 (8). Anal. calcd for $C_{18}H_{13}ClO_4$: C, 65.76; H, 3.99. Found: C, 65.73; H, 3.41.

3.1.2.8. 4,6-Dimethyl-2-oxo-2H-chromen-7-yl-4-chlorobenzoate (3j). ^{1}H NMR (400 MHz, $CDCl_3$): δ 8.23−8.11 (m, 2H), 7.60−7.51 (m, 2H), 7.50 (s, 1H), 7.19 (s, 1H), 6.29 (s, 1H), 2.45 (s, 3H), 2.30 (s, 3H). MS (EI): m/z (%) 328 ([M]$^+$, 7), 139 (100), 111 (15), 75 (3),44 (2). Anal. calcd for $C_{18}H_{13}ClO_4$: C, 65.76; H, 3.99. Found: C, 65.75; H, 3.43.

3.1.2.9. 4,6-Dimethyl-2-oxo-2H-chromen-7-yl-3,4-difluorobenzoate (3m). ^{1}H NMR (400 MHz, $CDCl_3$): δ 8.13−7.94 (m, 2H), 7.54 (d, J = 8.7 Hz, 1H), 7.34 (dd, J = 17.2, 8.9 Hz, 1H), 7.14 (d, J = 8.7 Hz, 1H), 6.31 (s, 1H), 2.47 (s, 3H), 2.33 (s, 3H). MS (EI): m/z (%) 330 ([M]$^+$, 7), 141 (100), 113 (16), 77 (3), 44 (4). Anal. calcd for $C_{18}H_{12}F_2O_4$: C, 65.46; H, 3.66. Found: C, 65.42; H, 3.64.

3.1.2.10. 4,6-Dimethyl-2-oxo-2H-chromen-7-yl-2,4-dichlorobenzoate (3p). ^{1}H NMR (400 MHz, $CDCl_3$): δ 8.07 (d, J = 8.5 Hz, 1H), 7.59 (d, J = 2.0 Hz, 1H), 7.50 (s, 1H), 7.42 (dd, J = 8.5, 2.0 Hz, 1H), 7.19 (s, 1H), 6.29 (s, 1H), 2.45 (d, J = 1.0 Hz, 3H), 2.33 (s, 3H). MS (EI): m/z (%) 362 ([M]$^+$, 3), 173 (100), 145 (11),108 (2), 77 (2). Anal. calcd for $C_{18}H_{12}Cl_2O_4$: C, 59.53; H, 3.33. Found: C, 59.51; H, 3.37.

3.1.2.11. 4,6-Dimethyl-2-oxo-2H-chromen-7-yl-3-(trifluoromethyl) Benzoate (3t). ^{1}H NMR (400 MHz, $CDCl_3$): δ 8.49 (s, 1H), 8.42 (d, J = 7.8 Hz, 1H), 7.95 (d, J = 7.8 Hz, 1H), 7.71 (t, J = 7.8 Hz, 1H), 7.52 (s, 1H), 7.20 (s, 1H), 6.30 (s, 1H), 2.46 (s, 3H), 2.31 (s, 3H). MS (EI): m/z (%) 362 ([M]$^+$, 10), 173 (100), 145 (26), 95 (22), 77 (1). Anal. calcd for $C_{19}H_{13}F_3O_4$: C, 62.99; H, 3.62. Found: C, 62.96; H, 3.59.

3.1.2.12. 4,6-Dimethyl-2-oxo-2H-chromen-7-yl-4-(trifluoromethyl) Benzoate (3u). ^{1}H NMR (400 MHz, $CDCl_3$): δ 8.36 (d, J = 8.2 Hz, 2H), 7.83 (d, J = 8.3 Hz, 2H), 7.55 (d, J = 8.7 Hz, 1H), 7.17 (d, J = 8.7 Hz, 1H), 6.32 (s, 1H), 2.47 (s, 3H), 2.34 (s, 3H). MS (EI): m/z (%) 362 ([M]$^+$, 5), 173 (100), 145 (26), 95 (2), 44 (2). Anal. calcd for $C_{19}H_{13}F_3O_4$: C, 62.99; H, 3.62. Found: C, 62.95; H, 3.64.

3.1.2.13. 4,6-Dimethyl-2-oxo-2H-chromen-7-yl-4-methoxybenzoate (3w). ^{1}H NMR (400 MHz, $CDCl_3$): δ 8.24−8.13 (m, 2H), 7.48 (s, 1H), 7.18 (s, 1H), 7.05−6.99 (m, 2H), 6.27 (s, 1H), 3.92 (s, 3H), 2.44 (s, 3H), 2.30 (s, 3H). MS (EI): m/z (%) 324 ([M]$^+$, 2), 135 (100), 107 (4), 77 (6), 44 (1). Anal. calcd for $C_{19}H_{16}O_5$: C, 70.36; H, 4.97. Found: C, 70.33; H, 4.98.

3.1.2.14. 4,6-Dimethyl-2-oxo-2H-chromen-7-yl-furan-2-carboxylate (3x). ^{1}H NMR (400 MHz, $CDCl_3$): δ 7.72 (m, 1H), 7.49 (s, 1H), 7.45 (d, J = 3.5 Hz, 1H), 7.19 (s, 1H), 6.69−6.58 (m, 1H), 6.28 (s, 1H), 2.44 (s, 3H), 2.31 (s, 3H). MS (EI): m/z (%) 284 ([M]$^+$, 17), 96 (6), 95 (100), 67 (2). Anal. calcd for $C_{16}H_{12}O_5$: C, 67.60; H, 4.25. Found: C, 67.64; H, 4.22.

3.1.2.15. 4,6-Dimethyl-2-oxo-2H-chromen-7-yl-thiophene-2-carboxylate (3y). ^{1}H NMR (400 MHz, $CDCl_3$): δ 8.03 (dd, J = 3.8, 1.1 Hz, 1H), 7.72 (dd, J = 5.0, 1.1 Hz, 1H), 7.48 (s, 1H), 7.22 (t, J = 4.4 Hz, 2H), 6.28 (s, 1H), 2.45 (s, 3H), 2.32 (s, 3H). MS (EI): m/z (%) 300 ([M]$^+$, 8), 161 (1), 111 (100), 83 (4), 77 (1). Anal. calcd for $C_{16}H_{12}O_4S$: C, 63.99; H, 4.03; S, 10.68. Found: C, 63.95; H, 4.04; S, 10.71.

3.1.2.16. 4,6-Dimethyl-2-oxo-2H-chromen-7-yl-1-naphthoate (3aa). ^{1}H NMR (400 MHz, $CDCl_3$): δ 9.04 (d, J = 8.6 Hz, 1H), 8.55 (dd, J = 7.3, 1.2 Hz, 1H), 8.16 (d, J = 8.2 Hz, 1H), 7.96 (d, J = 8.1 Hz, 1H), 7.67 (ddd, J = 18.0, 9.7, 6.3 Hz, 2H), 7.63−7.56 (m, 2H), 7.53 (s, 1H), 6.30 (s, 1H), 2.47 (s, 3H), 2.37 (s, 3H). MS (EI): m/z (%) 334 ([M]$^+$, 3), 155 (100), 127 (40), 65 (2), 44 (7). Anal. calcd for $C_{22}H_{16}O_4$: C, 76.73; H, 4.68. Found: C, 76.77; H, 4.65.

3.1.2.17. 4,6-Dimethyl-2-oxo-2H-chromen-7-yl-2-naphthoate (3bb). ^{1}H NMR (400 MHz, $CDCl_3$): δ 8.82 (s, 1H), 8.21 (dd, J = 8.6, 1.7 Hz, 1H), 8.05−7.91 (m, 3H), 7.72−7.58 (m, 2H), 7.52 (s, 1H), 7.25 (s, 1H), 6.29 (s, 1H), 2.46 (s, 3H), 2.35 (s, 3H). MS (EI): m/z (%) 344 ([M]$^+$, 6), 155 (100), 127 (45), 77 (2), 44 (5). Anal. calcd for $C_{22}H_{16}O_4$: C, 76.73; H, 4.68. Found: C, 76.71; H, 4.64.

3.1.2.18. 4,6-Dimethyl-2-oxo-2H-chromen-7-yl-cyclopropanecarboxylate (3cc). ^{1}H NMR (400 MHz, $CDCl_3$): δ 7.42 (s, 1H), 7.05 (s, 1H), 6.23 (s, 1H), 2.41 (s, 3H), 2.24 (s, 3H), 1.91−1.88 (m, 1H), 1.22−1.21 (m, 2H), 1.09−1.08 (m, 2H). MS (EI): m/z (%) 258 ([M]$^+$, 16), 190 (7), 162 (5),69 (100), 41 (13). Anal. calcd for $C_{15}H_{14}O_4$: C, 69.76; H, 5.46. Found: C, 69.77; H, 5.45.

3.1.3. Spectral Analysis of Target Compound I. 3.1.3.1. 5-Methyl-2-phenyl-7H-furo [3,2-g] Chromen-7-one (Ia). ^{1}H NMR (400 MHz, $CDCl_3$): δ 7.85 (d, J = 7.3 Hz, 2H), 7.75 (d, J = 1.7 Hz, 1H), 7.47 (t, J = 7.4 Hz, 3H), 7.40 (d, J = 7.4 Hz, 1H), 7.04 (s, 1H), 6.25 (s, 1H), 2.49 (s, 3H). ^{13}C NMR (100 MHz, $CDCl_3$): δ 160.95, 157.90, 152.20, 151.68, 150.19, 132.82, 132.19, 126.06, 126.02, 125.52, 117.91, 114.56, 108.24, 106.12, 103.21, 19.01. MS (EI): m/z (%) 276 ([M]$^+$, 100), 248 (36), 219 (7), 189 (9), 124 (12), 105 (29). Anal. calcd for $C_{18}H_{12}O_3$: C, 78.25; H, 4.38. Found: C, 78.22; H, 4.35.

3.1.3.2. 2-(2-Fluorophenyl)-5-methyl-7H-furo [3,2-g] Chromen-7-one (Ib). ^{1}H NMR (400 MHz, $CDCl_3$): δ 8.04 (dd, J = 8.4, 6.9 Hz, 1H), 7.82 (s, 1H), 7.50 (s, 1H), 7.37 (d, J

https://dx.doi.org/10.1021/acs.jafc.0c07237
J. Agric. Food Chem. 2021, 69, 1091−1106

= 7.3 Hz, 1H), 7.33−7.27 (m, 2H), 7.20 (dd, J = 11.4, 8.2 Hz, 1H), 6.29 (s, 1H), 2.52 (s, 3H). ^{13}C NMR (100 MHz, $CDCl_3$): δ 161.05, 158.36, 155.64, 152.65, 151.97, 130.19, 127.06, 126.62, 124.65, 118.11, 116.87, 116.52, 116.26, 116.05, 113.50, 106.07, 99.57, 19.18. MS (EI): m/z (%) 295 ([M + 1]$^+$, 14.25), 294 ([M]$^+$, 100), 266 (58.72), 265 (26.93), 237 (3.85), 236 (1.66), 209 (3.10), 207 (2.54), 189 (1.98), 133 (8.76), 123 (2.42). Anal. calcd for $C_{18}H_{11}FO_3$: C, 73.47; H, 3.77. Found: C, 73.48; H, 3.75.

3.1.3.3. 2-(3-Fluorophenyl)-5-methyl-7H-furo [3,2-g] Chromen-7-one (Ic). ^{1}H NMR (400 MHz, $CDCl_3$): δ 7.80 (s, 1H), 7.65 (d, J = 7.9 Hz, 1H), 7.58−7.53 (m, 1H), 7.50 (s, 1H), 7.45 (dd, J = 8.1, 5.8 Hz, 2H), 7.09 (s, 1H), 6.29 (s, 1H), 2.52 (s, 3H). ^{13}C NMR (100 MHz, $CDCl_3$): δ 160.96, 156.35, 152.53, 151.97, 132.08, 130.58, 128.46, 126.20, 120.71, 116.98, 116.33, 116.17, 115.95, 113.64, 112.11, 111.88, 101.81, 99.80, 19.17. MS (EI): m/z (%) 294 ([M]$^+$, 100), 266 (62), 237 (8), 207 (9), 133 (29), 104 (7), 95 (10). Anal. calcd for $C_{18}H_{11}FO_3$: C, 73.47; H, 3.77. Found: C, 73.46; H, 3.76.

3.1.3.4. 6-Chloro-2-(2-fluorophenyl)-5-methyl-7H-furo [3,2-g] Chromen-7-one (Ie). ^{1}H NMR (400 MHz, $CDCl_3$): δ 8.04 (td, J = 7.7, 1.8 Hz, 1H), 7.86 (s, 1H), 7.53 (s, 1H), 7.43−7.35 (m, 1H), 7.33−7.27 (m, 2H), 7.21 (ddd, J = 11.4, 8.2, 1.1 Hz, 1H), 2.69 (s, 3H). ^{13}C NMR (100 MHz, $CDCl_3$): δ 160.92, 157.21, 155.36, 152.35, 149.83, 148.01, 130.39, 127.13, 124.69, 119.35, 117.96, 116.79, 116.66, 116.31, 116.09, 106.01, 99.59, 16.68. MS (EI): m/z (%) 330 ([M + 1]$^+$, 25.78), 329 ([M]$^+$, 8.35), 328 ([M − 1]$^+$, 100), 300 (4.30), 265 (51.14), 207 (7.47), 181 (1.34), 163 (1.50), 150 (3.66), 133 (6.38), 122 (1.42), 118 (2.39), 108 (1.51), 104 (3.36), 94 (6.79). Anal. calcd for $C_{18}H_{10}ClFO_3$: C, 65.77; H, 3.07. Found: C, 65.78; H, 3.04.

3.1.3.5. 6-Chloro-2-(3-fluorophenyl)-5-methyl-7H-furo [3,2-g] Chromen-7-one (If). ^{1}H NMR (400 MHz, $CDCl_3$): δ 7.84 (s, 1H), 7.65 (d, J = 7.8 Hz, 1H), 7.56 (d, J = 9.7 Hz, 1H), 7.53 (s, 1H), 7.45 (d, J = 5.8 Hz, 1H), 7.11 (s, 2H), 2.69 (s, 3H). ^{13}C NMR (100 MHz, $CDCl_3$): δ 164.39, 161.93, 157.13, 156.05, 149.80, 147.90, 130.72, 126.76, 120.81, 119.48, 116.59, 116.35, 116.14, 112.19, 111.95, 101.76, 99.81, 16.68. MS (EI): m/z (%) 330 ([M + 1]$^+$, 33.58), 329 ([M]$^+$, 11.09), 328 ([M − 1]$^+$, 100), 300 (4.84), 265 (64.93), 237 (4.34), 207 (15.73), 183 (1.40), 164 (1.51), 150 (3.75), 132 (17.78). Anal. calcd for $C_{18}H_{10}ClFO_3$: C, 65.77; H, 3.07. Found: C, 65.75; H, 3.06.

3.1.3.6. 6-Chloro-2-(4-fluorophenyl)-5-methyl-7H-furo [3,2-g] Chromen-7-one (Ig). ^{1}H NMR (400 MHz, $CDCl_3$): δ 7.89−7.83 (m, 2H), 7.82 (s, 1H), 7.51 (s, 1H), 7.18 (t, J = 8.7 Hz, 2H), 7.02 (s, 1H), 2.69 (s, 3H). ^{13}C NMR (100 MHz, $CDCl_3$): δ 157.53, 157.22, 156.03, 149.57, 147.96, 140.19, 127.12, 127.04, 119.37, 116.63, 116.30, 116.26, 116.08, 100.41, 99.71, 16.68. MS (EI): m/z (%) 330 ([M + 1]$^+$, 17.18), 329 ([M]$^+$, 8.04), 328 ([M-1]$^+$, 100), 300 (2.65), 272 (1.34), 265 (51.21), 237 (5.26), 207 (8.14), 183 (1.41), 170 (1.00), 150 (3.22), 132 (19.02). Anal. calcd for $C_{18}H_{10}ClFO_3$: C, 65.77; H, 3.07. Found: C, 65.73; H, 3.10.

3.1.3.7. 2-(3-Chlorophenyl)-5-methyl-7H-furo [3,2-g] Chromen-7-one (Ii). ^{1}H NMR (400 MHz, $CDCl_3$): δ 7.78 (s, 1H), 7.73 (d, J = 8.5 Hz, 2H), 7.60 (d, J = 8.5 Hz, 2H), 7.49 (s, 1H), 7.07 (s, 1H), 6.29 (s, 1H), 2.52 (s, 3H). ^{13}C NMR (100 MHz, $CDCl_3$): δ 160.96, 156.95, 156.36, 152.52, 151.91, 132.19, 131.18, 129.88, 128.58, 126.49, 126.32, 123.32, 116.96, 116.18, 113.62, 101.30, 99.76, 19.16. MS (EI): m/z (%) 312 ([M]$^+$, 38), 310 (100), 282 (76), 276 (9), 254 (6), 219 (8), 189 (18), 141 (18). Anal. calcd for $C_{18}H_{11}ClO_3$: C, 69.58; H, 3.57. Found: C, 69.55; H, 3.56.

3.1.3.8. 2-(4-Chlorophenyl)-5-methyl-7H-furo [3,2-g] Chromen-7-one (Ij). ^{1}H NMR (400 MHz, $CDCl_3$): δ 7.81 (s, 1H), 7.79 (s, 2H), 7.49 (s, 1H), 7.45 (d, J = 8.6 Hz, 2H), 7.06 (s, 1H), 6.29 (s, 1H), 2.52 (s, 3H). ^{13}C NMR (100 MHz, $CDCl_3$): δ 161.00, 156.92, 156.35, 152.55, 151.87, 135.11, 129.25, 128.15, 126.34, 126.27, 116.93, 116.16, 113.60, 101.19, 99.75, 19.18. MS (EI): m/z (%) 312 ([M + 1H]$^+$, 31.34), 311 ([M]$^+$, 17.47), 310 ([M − 1]$^+$, 100), 284 (16.71), 283 (19.22), 282 (51.21), 281 (34.76), 254 (1.40), 219 (2.05), 189 (13.05), 176 (3.33), 141 (13.25), 109 (4.15), 94(15.02). Anal. calcd for $C_{18}H_{11}ClO_3$: C, 69.58; H, 3.57. Found: C, 69.57; H, 3.55.

3.1.3.9. 2-(3,4-Difluorophenyl)-5-methyl-7H-furo [3,2-g] Chromen-7-one (Im). ^{1}H NMR (400 MHz, $CDCl_3$): δ 7.69 (dd, J = 6.1, 5.0 Hz, 1H), 7.59 (s, 1H), 7.50 (dd, J = 29.9, 8.7 Hz, 2H), 7.33 (s, 1H), 7.30 (d, J = 8.3 Hz, 1H), 6.30 (s, 1H), 2.51 (s, 3H). ^{13}C NMR (100 MHz, $CDCl_3$): δ 160.69, 156.95, 154.87, 153.47, 147.72, 121.41, 121.13, 120.85, 118.58, 118.22, 118.04, 114.99, 114.35, 114.16, 113.11, 108.14, 99.35, 19.39. MS (EI): m/z (%) 312 ([M]$^+$, 100), 294 (1.11), 284 (97.00), 227 (2.92), 207 (3.67), 142 (10.52). Anal. calcd for $C_{18}H_{10}F_2O_3$: C, 69.23; H, 3.23. Found: C, 69.25; H, 3.20.

3.1.3.10. 2-(2,4-Dichlorophenyl)-5-methyl-7H-furo [3,2-g] Chromen-7-one (Ip). ^{1}H NMR (400 MHz, $CDCl_3$): δ 8.02 (d, J = 8.6 Hz, 1H), 7.86 (s, 1H), 7.60 (s, 1H), 7.55 (s, 1H), 7.50 (s, 1H), 7.41 (d, J = 8.4 Hz, 1H), 6.30 (s, 1H), 2.53 (s, 3H). ^{13}C NMR (100 MHz, $CDCl_3$): δ 160.92, 155.52, 153.02, 152.53, 152.25, 134.96, 131.92, 130.83, 129.66, 127.62, 126.76, 126.21, 117.04, 116.90, 113.66, 107.16, 99.57, 19.18. MS (EI): m/z (%) 346 ([M + 1]$^+$,66.15), 344 ([M − 1]$^+$, 100), 316 (48.88), 315 (21.20), 189 (15.02), 173 (4.81), 157 (10.57), 122 (7.26), 99 (2.27), 94 (15.76). Anal. calcd for $C_{18}H_{10}Cl_2O_3$: C, 62.63; H, 2.92. Found: C, 62.61; H, 2.94.

3.1.3.11. 5-Methyl-2-(3-(trifluoromethyl) phenyl)-7H-furo [3,2-g] Chromen-7-one (It). ^{1}H NMR (400 MHz, $CDCl_3$): δ 8.12 (s, 1H), 8.04 (d, J = 7.5 Hz, 1H), 7.82 (s, 1H), 7.67−7.58 (m, 2H), 7.53 (s, 1H), 7.17 (s, 1H), 6.30 (s, 1H), 2.53 (s, 3H). ^{13}C NMR (100 MHz, $CDCl_3$): δ 160.90, 156.43, 156.32, 152.48, 152.10, 131.47, 130.47, 129.55, 128.05, 126.10, 125.63, 125.24, 121.86, 117.11, 116.48, 113.74, 102.16, 99.88, 19.17.

3.1.3.12. 5-Methyl-2-(4-(trifluoromethyl) phenyl)-7H-furo [3,2-g] Chromen-7-one (Iu). ^{1}H NMR (400 MHz, $CDCl_3$): δ 7.98 (d, J = 8.2 Hz, 2H), 7.74 (d, J = 8.3 Hz, 2H), 7.56 (d, J = 8.6 Hz, 1H), 7.54−7.42 (m, 2H), 6.30 (s, 1H), 2.52 (s, 3H). ^{13}C NMR (100 MHz, $CDCl_3$): δ 160.64, 157.14, 155.36, 153.45, 147.86, 132.84, 130.68, 126.03, 125.99, 125.21, 121.19, 118.51, 114.99, 113.15, 108.24, 100.55, 19.38. MS (EI): m/z (%) 344 ([M]$^+$, 93.74), 316 (100), 288 (4.16), 259 (2.79), 233(2.54), 189 (4.01), 173 (4.24), 158 (5.51), 148 (4.12), 132 (1.90), 115 (1.77), 91 (2.04). Anal. calcd for $C_{19}H_{11}F_3O_3$: C, 66.28; H, 3.22. Found: C, 66.30; H, 3.23.

3.1.3.13. 2-(4-Methoxyphenyl)-5-methyl-7H-furo [3,2-g] Chromen-7-one (Iw). ^{1}H NMR (400 MHz, $CDCl_3$): δ 7.81 (d, J = 8.8 Hz, 2H), 7.75 (s, 1H), 7.48 (s, 1H), 7.00 (d, J = 8.8 Hz, 2H), 6.93 (s, 1H), 6.28 (s, 1H), 3.88 (s, 3H), 2.52 (s, 3H). ^{13}C NMR (100 MHz, $CDCl_3$): δ 156.27, 154.05, 152.74, 151.44, 146.46, 126.86, 126.62, 122.45, 120.47, 116.63, 115.51, 114.44, 113.32, 99.57, 99.00, 55.43, 19.20. MS (EI): m/z (%) 278 ([M − 28]$^+$,37.16), 277 (100), 201 (13.37), 199 (15.85), 183 (15.75), 171 (2.53), 152 (11.53), 128 (2.21), 95 (1.96),

https://dx.doi.org/10.1021/acs.jafc.0c07237
J. Agric. Food Chem. 2021, 69, 1091−1106

77 (21.53), Anal. calcd for $C_{19}H_{14}O_4$: C, 74.50; H, 4.61. Found: C, 74.48; H, 4.65.

3.1.3.14. 2-(Furan-2-yl)-5-methyl-7H-furo [3,2-g] Chromen-7-one (Ix). ^{1}H NMR (400 MHz, $CDCl_3$): δ 7.78 (s, 1H), 7.55 (s, 1H), 7.47 (s, 1H), 6.95 (s, 1H), 6.86 (d, J = 3.4 Hz, 1H), 6.56 (s, 1H), 6.29 (s, 1H), 2.52 (s, 3H). ^{13}C NMR (100 MHz, $CDCl_3$): δ 161.04, 158.11, 152.60, 151.78, 143.62, 126.07, 119.24, 116.07, 113.54, 112.78, 112.18, 111.92, 108.72, 100.35, 99.71, 19.19. MS (EI): m/z (%) 266([M]$^+$, 100), 238 (44.49), 237 (29.10), 209 (9.47), 181 (5.65), 152 (11.79), 139 (2.37), 119 (11.82), 104 (2.28), 91 (6.12), 76 (10.17). Anal. calcd for $C_{16}H_{10}O_4$: C, 72.18; H, 3.79. Found: C, 72.14; H, 3.76.

3.1.3.15. 5-Methyl-2-(thiophen-2-yl)-7H-furo [3,2-g] Chromen-7-one (Iy). ^{1}H NMR (400 MHz, $CDCl_3$): δ 7.74 (s, 1H), 7.53 (d, J = 3.6 Hz, 1H), 7.47 (s, 1H), 7.40 (d, J = 5.0 Hz, 1H), 7.18−7.08 (m, 1H), 6.90 (s, 1H), 6.28 (s, 1H), 2.51 (s, 3H). ^{13}C NMR (100 MHz, $CDCl_3$): δ 161.06, 156.07, 153.37, 152.58, 151.73, 132.33, 128.09, 126.65, 126.44, 125.42, 116.89, 115.76, 113.52, 100.38, 99.66, 19.18. MS (EI): m/z (%) 282 ([M]$^+$, 100), 254 (47.83), 253 (21.80), 223 (2.31), 197 (4.13), 171 (1.41), 158 (1.80), 152 (1.37), 127 (12.93), 111 (9.69). Anal. calcd for $C_{16}H_{10}O_3S$: C, 68.07; H, 3.57; S, 11.36. Found: C, 68.04; H, 3.60; S, 11.33.

3.1.3.16. 5-Methyl-2-(naphthalen-1-yl)-7H-furo [3,2-g] Chromen-7-one (Iaa). ^{1}H NMR (400 MHz, $CDCl_3$): δ 8.44 (d, J = 8.0 Hz, 1H), 8.01−7.91 (m, 3H), 7.88 (s, 1H), 7.65−7.53 (m, 4H), 7.15 (d, J = 0.9 Hz, 1H), 6.31 (s, 1H), 2.55 (s, 3H). ^{13}C NMR (100 MHz, $CDCl_3$): δ 161.13, 157.77, 156.41, 152.66, 151.77, 133.99, 130.56, 130.15, 128.81, 127.54, 127.35, 127.17, 126.37, 126.32, 125.28, 125.17, 116.78, 116.17, 113.51, 105.41, 99.77, 19.20. MS (EI): m/z (%) 326 ([M]$^+$, 100), 314 (1.52), 298 (21.28), 297 (11.38), 239 (5.33), 226 (1.24), 200 (1.19), 155 (4.65), 149 (10.89), 127 (3.53), 120 (2.70), 113 (2.25), 91 (9.42). Anal. calcd for $C_{22}H_{14}O_3$: C, 80.97; H, 4.32. Found: C, 80.96; H, 4.34.

3.1.3.17. 5-Methyl-2-(naphthalen-2-yl)-7H-furo [3,2-g] Chromen-7-one (Ibb). ^{1}H NMR (400 MHz, $CDCl_3$): δ 7.53 (d, J = 3.6 Hz, 1H), 7.51 (s, 1H), 7.49 (s, 1H), 7.45 (s, 1H), 7.43 (s, 1H), 7.40 (dd, J = 5.0, 1.0 Hz, 1H), 7.20 (s, 1H), 7.15 (s, 1H), 7.14 (d, J = 1.3 Hz, 1H), 7.13 (s, 1H), 6.28 (s, 1H), 2.50 (s, 3H). ^{13}C NMR (100 MHz, $CDCl_3$): δ 160.79, 156.58, 153.49, 152.45, 147.46, 132.25, 128.08, 126.69, 125.48, 120.32, 118.71, 118.62, 114.95, 114.83, 113.00, 108.00, 98.27, 19.38. MS (EI): m/z (%) 283 ([M − 43]$^+$,14.09), 282 (100), 254 (66.68), 253 (19.41), 225 (4.10), 197 (4.43), 171 (4.23), 165 (1.86), 141 (1.05), 126 (10.38), 115 (1.74). Anal. calcd for $C_{22}H_{14}O_3$: C, 80.97; H, 4.32. Found: C, 80.95; H, 4.29.

3.1.3.18. 2-Cyclopropyl-5-methyl-7H-furo [3,2-g] Chromen-7-one (Icc). ^{1}H NMR (400 MHz, $CDCl_3$): δ 7.63 (s, 1H), 7.34 (s, 1H), 6.41 (s, 1H), 6.25 (s, 1H), 2.49 (s, 3H), 2.09−1.96 (m, 1H), 1.14−0.89 (m, 4H). ^{13}C NMR (101 MHz, $CDCl_3$): δ 162.77, 161.37, 155.83, 152.85, 150.98, 126.51, 116.20, 114.75, 113.11, 99.98, 99.25, 19.18, 9.44, 7.53. MS (EI): m/z (%) 240 ([M]$^+$, 100), 239 (7.03), 234 (1.25), 212 (29.34), 211 (26.01), 197 (1.34), 185 (12.60), 169 (1.09), 153 (1.86), 139 (1.89), 127 (2.26), 115 (8.64), 105 (8.64), 92 (2.41). Anal. calcd for $C_{15}H_{12}O_3$: C, 74.99; H, 5.03. Found: C, 75.02; H, 5.06.

NMR results showed that the chemical shift of the 3-position hydrogen atom of coumarin in target compound I was 6.29 ppm nearby, that of 4-methyl was 2.50 ppm nearby, and that of a furan ring was 7.09 ppm nearby. If the 3-position hydrogen atom was replaced by chlorine, the peak near 6.30 ppm disappeared, corresponding 4-methyl was affected by 3-position chlorine, and the chemical shift moved to the high field, at 2.63 ppm. The mass spectra show that the molecular ion peaks of these compounds were abundant, and some of them were basic peaks, indicating that the molecular ion peaks of these substances are stable.

3.1.4. Insecticidal Activity of Target Compound I. The data in Table 3 indicate that under light exposure, the activities of compounds Ia, Ic, Ie, Ig, Ij, Ip, Iw, Ix, Iy, and Icc against *Culex pipiens pallens* were more than 90%; especially, the activities of Ij, Iw, and Iy were 100%, which were equivalent to the activity of standard control alpha-terthienyl (α-T). In the dark, the activities of Ic, Ie, Ig, Ij, Ip, Iw, Ix, Iy, and Icc against *Culex pipiens pallens* were more than 80%. Among them, the activity of Ij was 100%, but the activity of Ia was only 21.67%, while the activity of the standard control α-T was 1.67%. It showed that these compounds had photosensitive activity, but the photosensitive activity was lower than that of α-T.

Table 3. Photochemical Insecticidal Effect of Target Compound I[a]

	corrected mortality of mosquito larvae (%)	
no.	light group	dark group
Ia	90.00 ± 3.60 e	21.67 ± 1.84 i
Ib	18.33 ± 1.52 f	23.33 ± 2.77 h
Ic	98.33 ± 3.06 b	98.33 ± 1.63 b
Ie	98.33 ± 3.05 b	90.00 ± 2.17 d
If	6.67 ± 1.23 g	0.00 l
Ig	91.67 ± 3.19 d	85.00 ± 2.80 e
Ij	100.00 a	100.00 a
Im	1.67 ± 1.62 j	0.00 l
Ip	93.33 ± 0.12 c	91.67 ± 1.98 c
Iu	5.00 ± 1.79 h	3.33 ± 0.09 j
Iw	100.00 a	90.00 ± 2.15 d
Ix	98.33 ± 2.62 b	81.67 ± 2.74 f
Iy	100.00 a	80.00 ± 2.56 g
Iaa	3.33 ± 0.05 i	3.33 ± 0.06 j
Icc	93.33 ± 1.26 c	80.00 ± 3.79 g
α-T	100.00 a	1.67 ± 1.62 k

[a]Note: Data are presented as the mean ± SD of at least three independent experiments. Different lowercase letters indicate a 0.05 level difference in p.

3.2. Toxicity of Iy to *A. aegypti* Larvae. The insecticidal activity test identified Iy as a highly active compound. Because its activity was 100% in light and 80% in the dark (Table 3), Iy was selected for further experiments with *A. aegypti*. After a 48 h treatment with Iy, the LC_{25}, LC_{50}, and LC_{75} of the compound in *A. aegypti* larvae were 53.96, 64.99, and 78.27 mg/L, respectively (Table 4). In the follow-up test, 0, 54, 65, and 78 mg/L were used as control, low, medium, and high concentrations, respectively, to further assess the effects of Iy

Table 4. Toxic Effects of Iy on the Larvae of *A. aegypti*[a]

toxicity	Iy (mg/L)
LC_{25}	53.96 ± 0.58*
LC_{50}	64.99 ± 0.15*
LC_{75}	78.27 ± 1.02*

[a]LC, lethal concentration. *p < 0.05 compared with the control.

https://dx.doi.org/10.1021/acs.jafc.0c07237
J. Agric. Food Chem. 2021, 69, 1091−1106

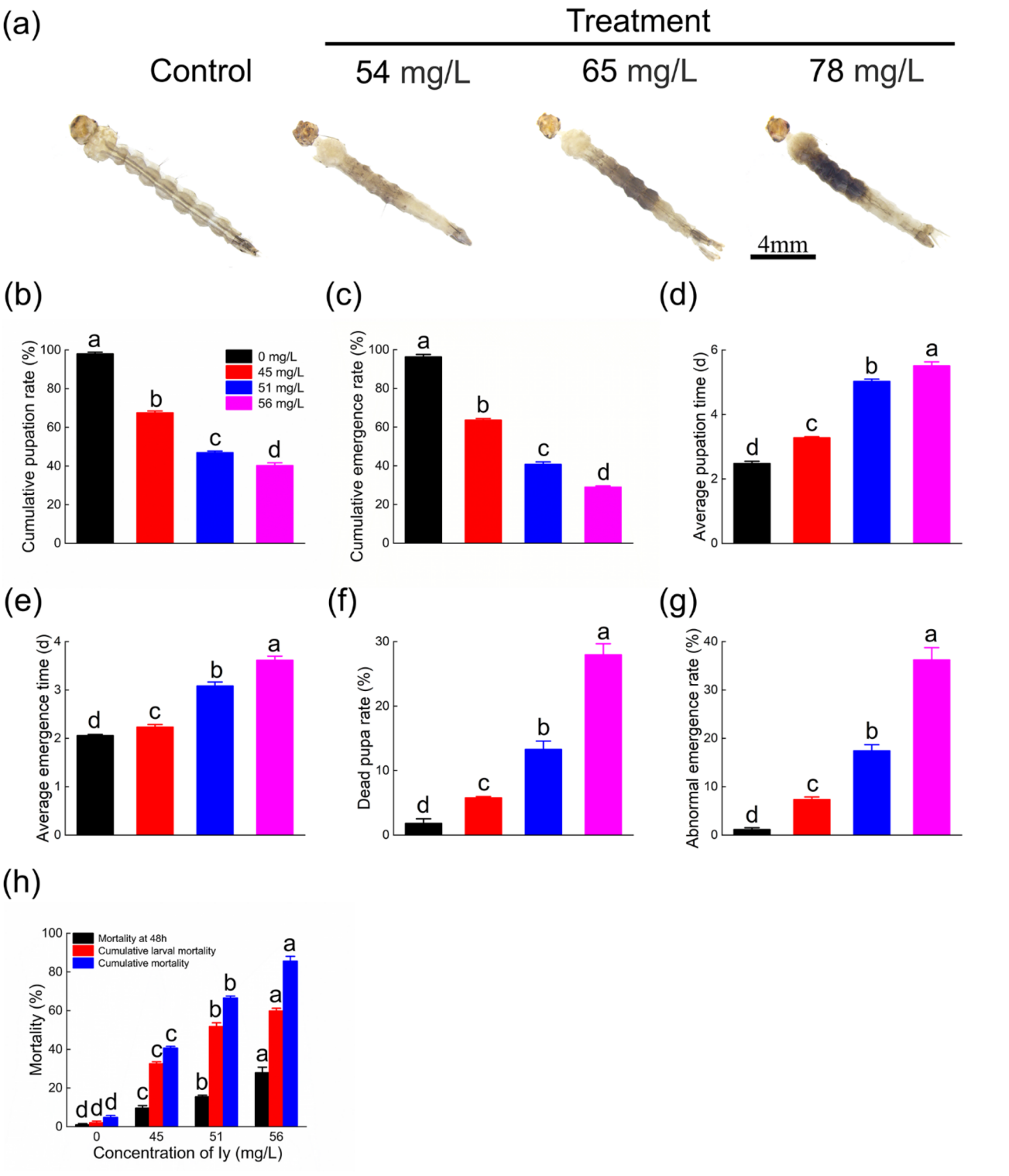

Figure 1. Effect of Iy on developmental parameters of *A. aegypti*. (a) Observation of poisoning symptoms in *A. aegypti* larvae (magnification, 2.5×; scale, 4 μm). (b) Cumulative pupation rate. (c) Cumulative emergence rate. (d) Average pupation time. (e) Average emergence time. (f) Dead pupa rate. (g) Abnormal emergence rate. (h) Mortality of *A. aegypti*. Data are presented as the mean ± SD of at least three independent experiments. Different lowercase letters indicate a 0.05 level difference in *p*.

on *A. aegypti* larvae, including the poisoning symptoms (Figure 1a). *A. aegypti* larvae were exposed to different Iy concentrations in the dark. After the light treatment, the Iy-exposed groups displayed different degrees of toxic reactions, and the activity of the larvae was increased during the initial period, especially at the medium and high concentration of Iy. After 48 h observation, the exposed larvae were weakened, and they swam up and down spasmodically after being touched by the needle. Most of the dead larvae were in a rigid state with a black abdomen, and their color was deepened at the higher Iy concentrations. Neither the blank control group nor the solvent control group exhibited toxic symptoms.

https://dx.doi.org/10.1021/acs.jafc.0c07237
J. Agric. Food Chem. 2021, 69, 1091−1106

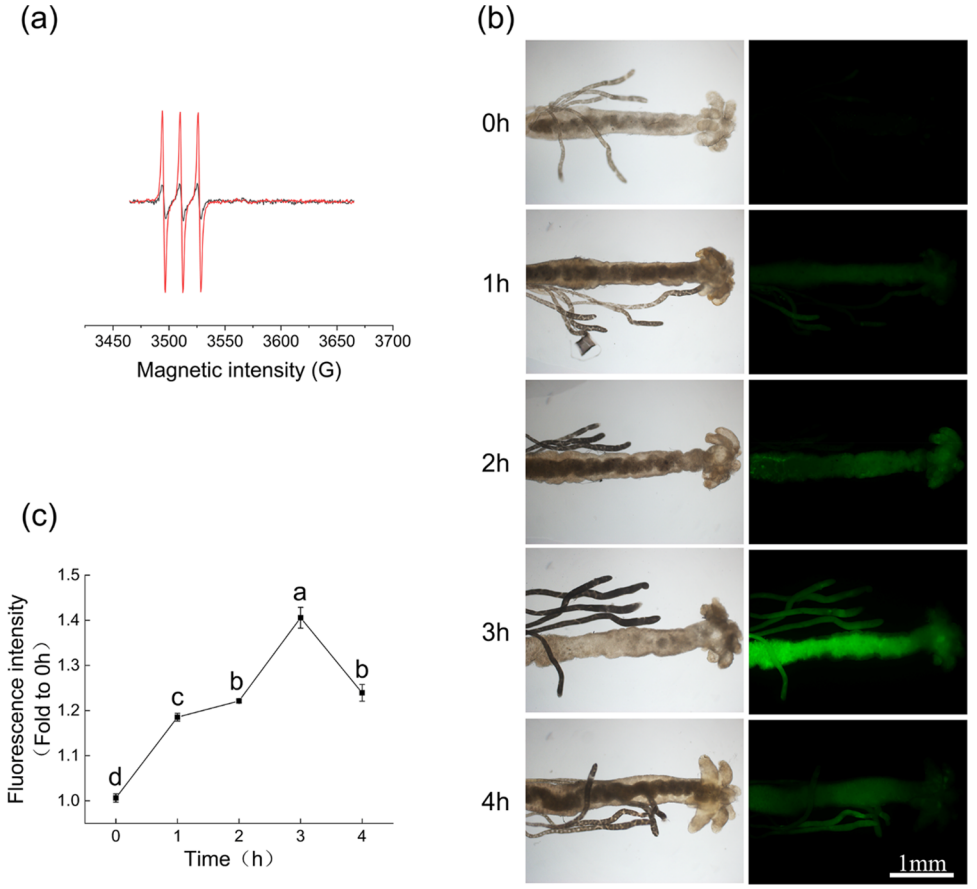

Figure 2. Effect of Iy on ROS production. (a) Detection of $^1O_2$. (b) Qualitative observation of ROS (magnification, 10×; scale, 1 mm). (c) Quantitative determination of ROS. Data are presented as the mean ± SD of at least three independent experiments. Different lowercase letters indicate a 0.05 level difference in *p*.

3.3. Iy Has an Obvious Post-Lethal Effect on *A. aegypti*. After treatment with different sublethal Iy concentrations for 48 h, the cumulative pupation rate and emergence rate were significantly reduced (Figure 1b,c, $P < 0.05$), and the pupation time and emergence time were significantly prolonged (Figure 1d,e, $P < 0.05$), compared with those in the control group. Thus, the survival and development of *A. aegypti* larvae were affected by Iy exposure. Furthermore, throughout the development from the pupa to the eclosion stage, the dead pupa rate and abnormal emergence rate were also increased (Figure 1f,g). The cumulative mortality of the whole development period was 8.5, 13.9, and 17.8 times higher in the low, medium, and high Iy groups than in the control group (Figure 1h, $P < 0.05$). These results indicated that Iy had an obvious post-lethal effect on *A. aegypti* at different developmental stages.

3.4. Iy Induces Cellular ROS Production. When the mixed solution was exposed to 365 nm black light for 30 min, an ESR spectrum was recorded (Figure 2a) that was consistent with the ESR signal, which showed that the presence of Iy in the system triggered the light-dependent $^1O_2$ increase, indicating the induction of ROS production.[40] The analysis of the qualitative observations identified a weak level of fluorescence at 0 h, which was gradually increased after 1 and 2 h of light treatment and significantly enhanced after 3 h. At the latter time point, obvious green fluorescence was observed in the digestive organs, including the gastric caeca, midgut, and Malpighian tubules (Figure 2b). However, there was a decline in fluorescence after 4 h of light treatment. The quantitative analysis detected a statistically significant ROS burst after 3 h of light treatment, which was 1.41 times higher than the 0 h ROS level (Figure 2c, $P < 0.05$), which was consistent with the qualitative observation. Combined with the observation of poisoning symptoms, these results suggested that the midgut may be a potential site for Iy activity.

3.5. Mitochondrial Dysfunction of Midgut Cells Induced by Iy. The origin of ROS is related to mitochondria. Therefore, to evaluate the effect of Iy on mitochondria, TEM was used to analyze their morphology (Figure 3a). The structure of the control group mitochondria was intact, and their membrane and cristae were clearly visible. In contrast, the membrane and cristae of the Iy treatment group mitochondria were fuzzy, and there were vacuoles, suggesting that the structural integrity of the mitochondria was compromised.

Damage of mitochondria will inevitably affect their function. Therefore, we measured the enzymatic activities of respiratory complex and TCA cycle components in midgut cell mitochondria. All examined enzyme activities were increased in the low Iy group but significantly inhibited in the high Iy group (Figure 3). At the main ROS production sites specifically,[41] the activities of the respiratory complex I and III enzymes were decreased by 35.19 and 59.57%, respectively, compared with those in the control group (Figure 3b,d, $P < 0.05$). The ETC and TCA cycle enzymes were inhibited by Iy, which inevitably affected energy production. The ATP content

https://dx.doi.org/10.1021/acs.jafc.0c07237
J. Agric. Food Chem. 2021, 69, 1091−1106

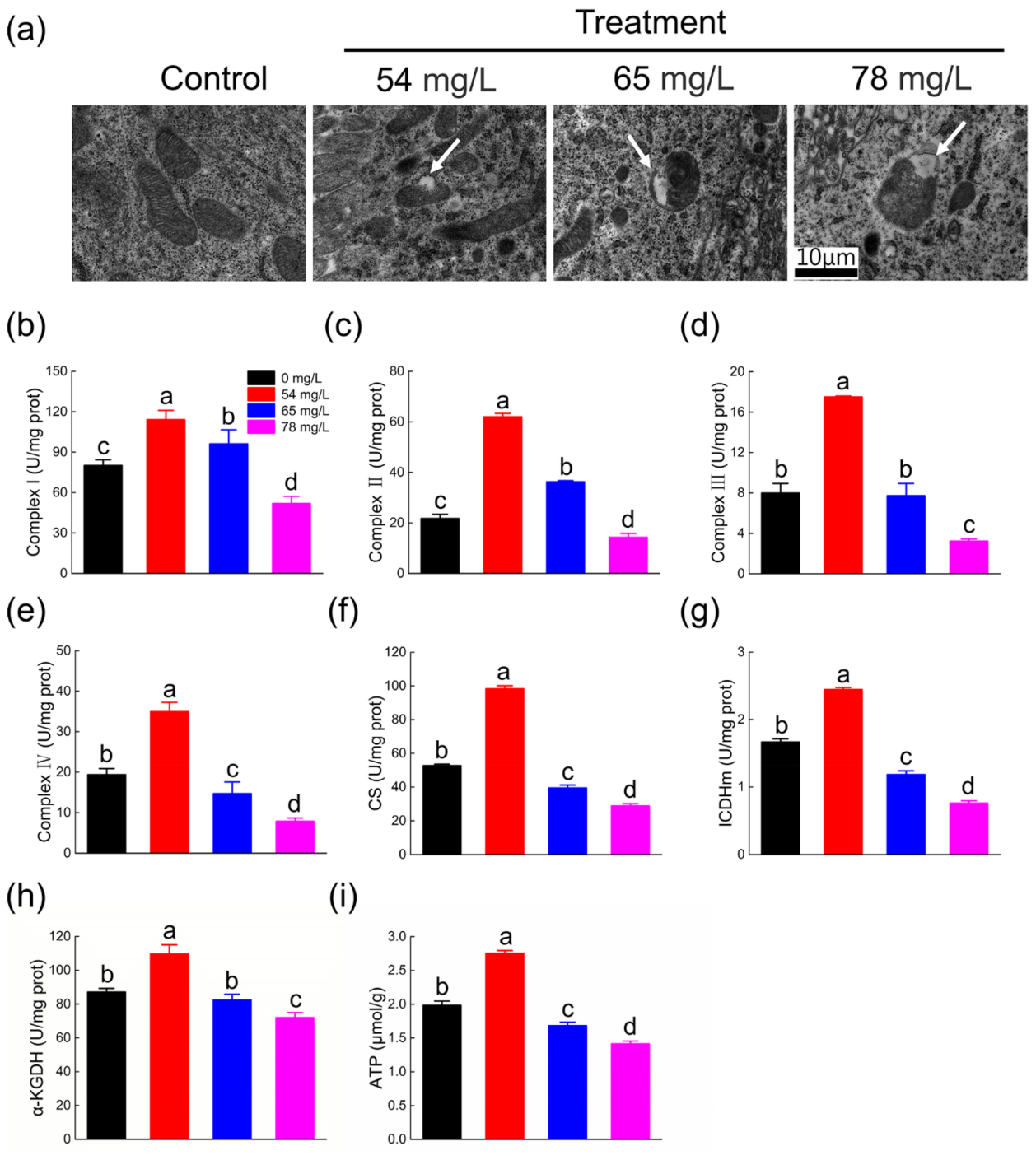

Figure 3. Effect of Iy on mitochondrial indicators of midgut cells. (a) Observation of the structure of mitochondria (magnification, 10000×; scale, 10 μm). (b) Activity of complex I. (c) Activity of complex II. (d) Activity of complex III. (e) Activity of complex IV. (f) Activity of CS. (g) Activity of ICDHm. (h) Activity of α-KGDH. (i) Content of ATP. Data are presented as the mean ± SD of at least three independent experiments. Different lowercase letters indicate a 0.05 level difference in p.

was significantly lower in the high Iy group than in the control group (Figure 3i, $P < 0.05$).

MMP changes were detected by JC-1 staining. JC-1 aggregates with strong red fluorescence were observed in the midgut cells of the control group (Figure 4a). The superposition of fluorescence images showed that the increase in the Iy concentration was associated with a significant increase in the green-to-red fluorescence ratio (Figure 4b, $P < 0.05$). Thus, the increase in the Iy concentration damaged the mitochondria, inhibited mitochondrial enzyme activities, blocked energy synthesis, and lowered MMP, resulting in mitochondrial dysfunction.

3.6. The Oxidative Stress in Midgut Cells Was Aggravated by Iy. The damaged mitochondria leaked ETC electrons and continuously produced ROS, which is known to cause oxidative stress. We found that the activities of SOD and CAT were increased in the low Iy group but inhibited in the medium and high Iy groups (Figure 5a,b, $P < 0.05$). High Iy concentration inhibited the activities of GR and GPx (Figure 5c,d, $P < 0.05$). By increasing the activity of antioxidant

https://dx.doi.org/10.1021/acs.jafc.0c07237
J. Agric. Food Chem. 2021, 69, 1091−1106

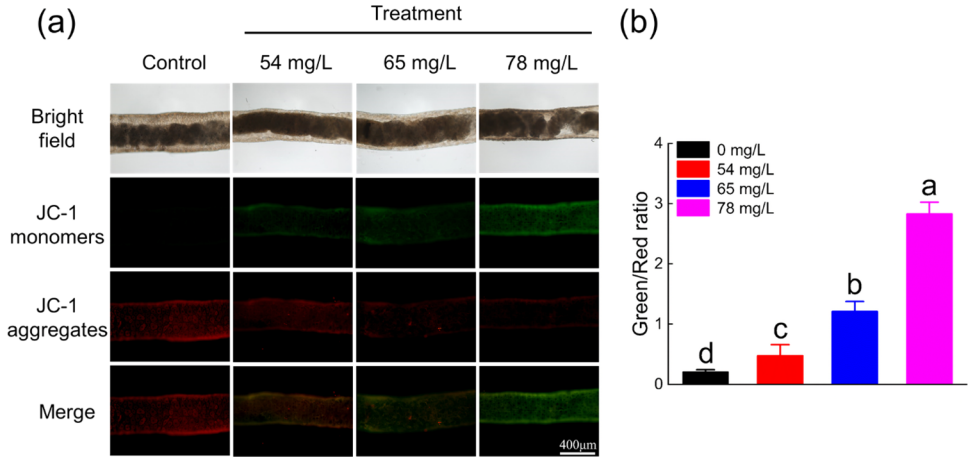

Figure 4. Effect of Iy on mitochondrial membrane potential of midgut cells. (a) Changes of mitochondrial membrane potential observed by a fluorescence microscope (magnification, 25×; scale, 400 μm). (b) Quantitative analysis of the mean green (JC-1 monomers)/red (JC-1 aggregates) fluorescence intensity ratio. Data are presented as the mean ± SD of at least three independent experiments. Different lowercase letters indicate a 0.05 level difference in p.

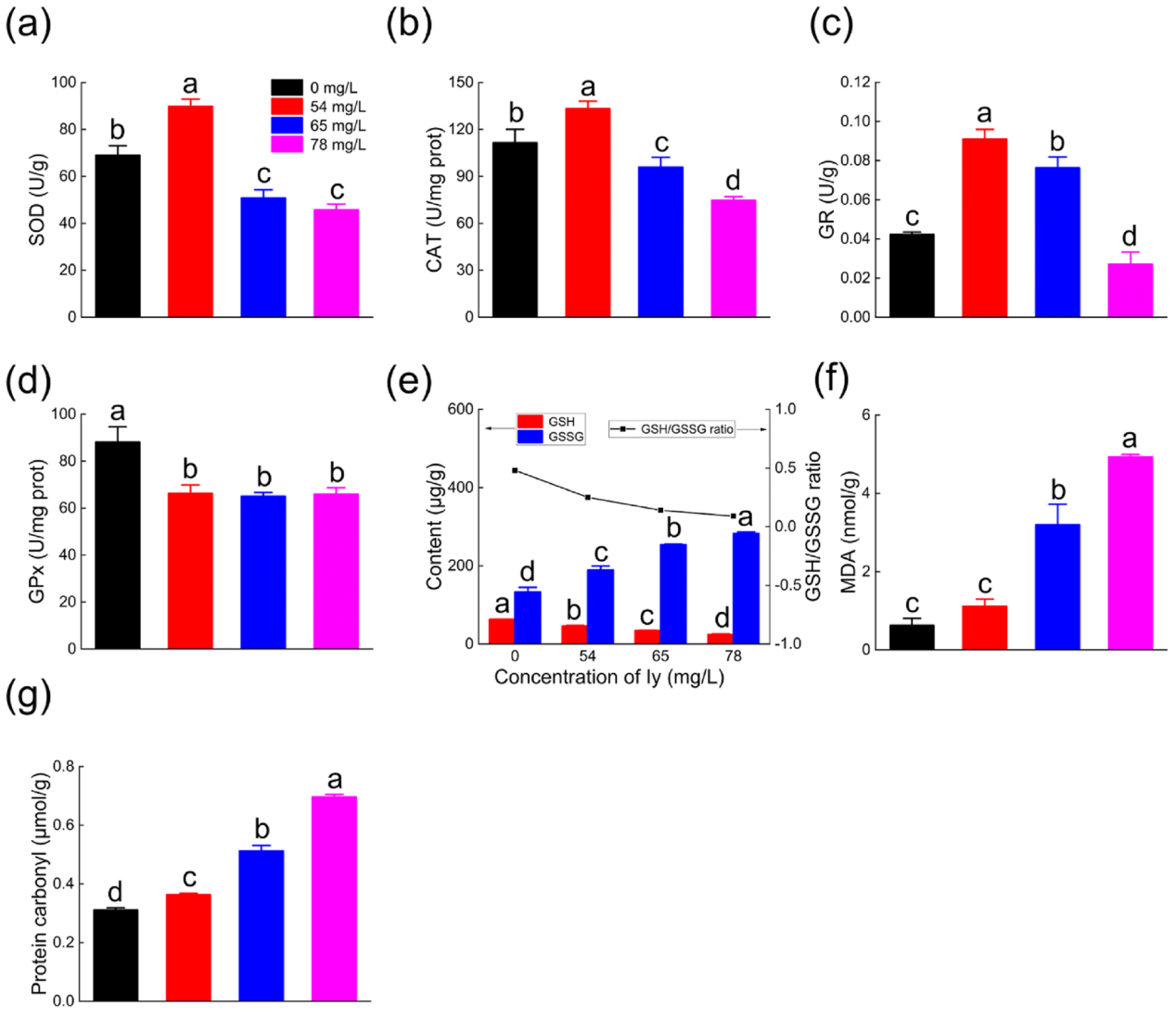

Figure 5. Effect of Iy on oxidative stress indicators of midgut cells. (a) Activity of SOD. (b) Activity of CAT. (c) Activity of GR. (d) Activity of GPx. (e) Content of GSH and GSSG and the GSH/GSSG ratio. (f) Content of MDA. (g) Content of protein carbonyls. Data are presented as the mean ± SD of at least three independent experiments. Different lowercase letters indicate a 0.05 level difference in p.

https://dx.doi.org/10.1021/acs.jafc.0c07237
J. Agric. Food Chem. 2021, 69, 1091−1106

enzymes, the balance of the antioxidant system was maintained in midgut cells exposed to a low ROS level. However, at higher Iy concentrations, the antioxidant system was out of balance, and the antioxidant enzyme activity was inhibited. In the presence of Iy, GSH was continuously consumed, the GSH/GSSG ratio was decreased (Figure 5e), the redox balance in midgut cells was diminished, the MDA and protein carbonyl levels were significantly increased (Figure 5f,g, $P < 0.05$), and the degree of oxidative damage was gradually increased.

Oxidative damage was easily detected by histopathological evaluation (Figure 6a,b). The midgut tissue, going from inside to outside, consists of the endo-peritrophic space, peritrophic membrane, and ecto-peritrophic space, and the epithelial cells were covered with microvilli.[37,42] In the control group, the midgut epithelial cells were intact and orderly arranged, the nucleocytoplasmic staining generated strong signals, and the striated border and peritrophic membrane were not broken. In contrast, under Iy treatment, the midgut tissues were damaged at varying degrees, the striated border was diminished, the cells were swollen, and there were instances of vacuolation and cell disintegration, associated with the appearance of intercellular space and midgut disruption. Orderly arranged microvilli were not detectable by TEM (Figure 6c).

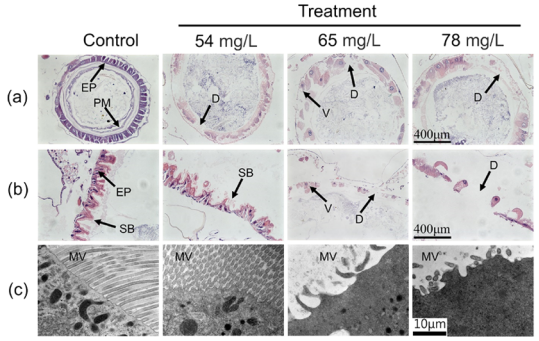

Figure 6. Histological and ultrastructural analysis of the midgut. (a) Structure of the midgut observed by transection (magnification, 40×; scale, 400 μm; EP, epithelial cell; PM, peritrophic membrane; D, cell disintegration; V, cell vacuolization). (b) Structure of the midgut observed by a longitudinal section (magnification, 40×; scale, 400 μm; SB, striated border). (c) Observation of microvilli (magnification, 10000×; scale, 10 μm; MV, microvilli).

3.7. Intestinal Shielding Dysfunction in *A. aegypti* Larvae Caused by Iy. The destruction of the intestinal structure appeared to affect the intestinal shielding function. Based on this assumption, the permeability of the peritrophic membrane was tested. When the peritrophic membrane was destroyed, (FITC)-dextran will exude from the intestine. Iy treatment was associated with increased fluorescence intensity and intestinal permeability, compared with those in the control group (Figure 7a). We also measured the level of chitin as the main component of the peritrophic membrane. Chitin can be affected when the peritrophic membrane is damaged.[43] The chitin level was significantly lower in each Iy group than in the control group (Figure 7b, $P < 0.05$). The increase in Iy concentration decreased the chitin level and damaged the peritrophic membrane.

3.8. Midgut Cell Apoptosis Induced by Iy. Because ROS accumulation can induce apoptosis, we measured the expression of apoptosis-related genes to assess the apoptosis status of midgut cells. Iy treatment increased the expression levels of *AeDronc*, *AeCaspase7*, and *AeCaspase8*, which were significantly upregulated in the high Iy group (Figure 8a–c, $P < 0.05$). Although the expression of the negative regulatory gene *AeIAP1* was increased, the elevated expression of the antagonist *AeMichelob_x* diminished the inhibition by *AeIAP1* and induced cell apoptosis (Figure 8d,e).

Apoptosis-specific staining was applied. The Hoechst 33342 stain densely labeled the nuclei of midgut cells treated with Iy (Figure 8f). The TUNEL staining detected broken genomic DNA in the midgut cells. The terminal deoxynucleotidyl transferase (TDT) added FITC-conjugated dUTP to exposed 3′-OH groups, which clearly labeled apoptotic spots (Figure 8g). The TEM analysis indicated that Iy treatment was associated with karyopyknosis (Figure 8h). Overall, these results suggested that Iy induced apoptosis in midgut cells.

4. DISCUSSION

The viral diseases transmitted by *A. aegypti* pose a threat to human health on a global scale. Furanocoumarin possesses photosensitive activity and has various pharmacological properties. In this study, we newly designed and synthesized 2-arylfuranocoumarin derivatives, including Iy, which we investigated for photoactivated toxicity in *A. aegypti*.

Specifically, Iy was activated by ultraviolet light to produce singlet oxygen, which induced ROS production in body cells. Our combined qualitative and quantitative ROS analysis identified the gastric caeca, midgut, and Malpighian tubules as sites with high ROS production. By monitoring the

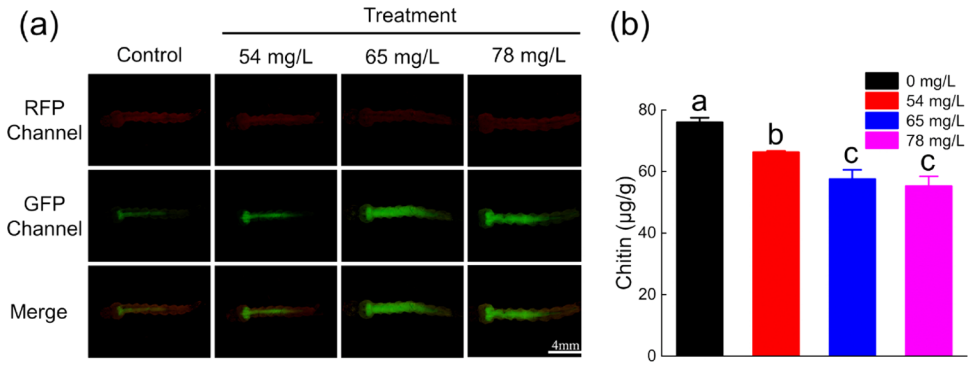

Figure 7. Effect of Iy on intestinal barrier dysfunction. (a) Detection of peritrophic membrane permeability (magnification, 2.5×; scale, 4 mm). (b) Detection of chitin content. Data are presented as the mean ± SD of at least three independent experiments. Different lowercase letters indicate a 0.05 level difference in *p*.

https://dx.doi.org/10.1021/acs.jafc.0c07237
J. Agric. Food Chem. 2021, 69, 1091−1106

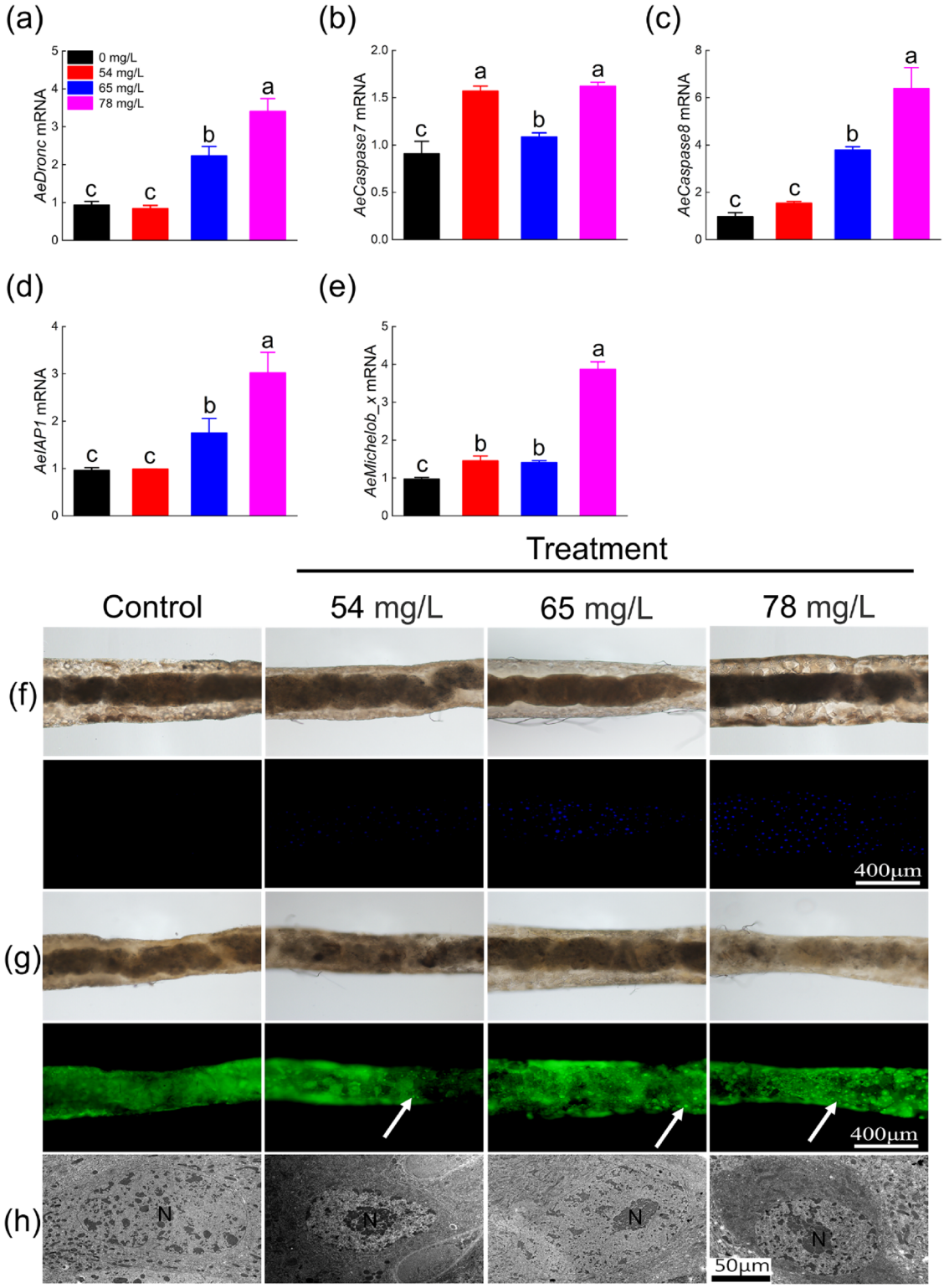

Figure 8. Effect of Iy on apoptosis of midgut cells. (a) Relative expression of *AeDronc* mRNA. (b) Relative expression of *AeCaspase7* mRNA. (c) Relative expression of *AeCaspase8* mRNA. (d) Relative expression of *AeIAP1* mRNA. (e) Relative expression of *AeMichelob_x* mRNA. (f) Hoechst 33342 staining. (g) TUNEL staining (magnification, 25×; scale, 400 μm). (h) Observation of the nucleus structure (magnification, 1500×; scale, 50 μm; N, nucleolus). Data are presented as the mean ± SD of at least three independent experiments. Different lowercase letters indicate a 0.05 level difference in *p*.

poisoning symptoms, we found that the abdomen of the *A. aegypti* larvae was blackened, suggesting that the site of Iy action in the larvae could be the midgut. In general, ROS is mainly generated by the ETC, and mitochondria not only produce ROS, but they are also targeted by these antioxidants.[44] The mitochondria were damaged by the Iy treatment, and the enzyme activities of ETC complexes were inhibited at different degrees, which especially applied to the

https://dx.doi.org/10.1021/acs.jafc.0c07237
J. Agric. Food Chem. 2021, 69, 1091−1106

respiratory complex III enzymes. Some earlier studies showed that a respiratory complex II key enzyme, which connects the ETC to the TCA, can also be a site of ROS production.[15,45,46] The activities of key enzymes in the TCA cycle are also inhibited by Iy in varying degrees. Interestingly, some studies have shown that α-KGDH can also participate in the production of ROS.[47,48] Furthermore, the function of mitochondria is highly dependent on MMP as a critical parameter for the real-time state of mitochondria, which plays an important role in maintaining biosynthesis and apoptosis.[49−51] Therefore, it was speculated that the decrease in MMP might play a key role in inducing apoptosis. The decrease in MMP leads to the dysfunction of mitochondria and promotes the continuous production of ROS in midgut cells.

The cells have an efficient antioxidant system, which can rapidly remove ROS. At a low level of ROS stimulation, the cells start the repair function, preventing ROS from reacting with lipids and proteins,[52,53] which causes oxidative damage. Thus, the increase in antioxidant enzyme activity at low ROS concentrations blocks further damage. However, mitochondrial dysfunction leads to continuous ROS production. When it exceeds the tolerance range of the intracellular antioxidant system, it will cause oxidative damage to the cells, which is associated with a gradual decrease in the GSH/GSSG ratio, indicating that the intracellular antioxidant system is out of balance. Histopathological changes in Iy-treated larvae indicated substantial midgut damage, increased intestinal permeability, and a decreased chitin content, which provided evidence that the intestinal shielding function was impaired.

However, the excessive ROS production caused by Iy-induced damage of the mitochondria cannot be rapidly eliminated in time due to the impairment of the intracellular antioxidant system by Iy. Thus, Iy treatment promoted the accumulation of ROS, which led to the induction of apoptosis. *AeDronc* was induced as an apoptosis initiator gene, which significantly upregulated and activated the downstream effect caspases, indicating that apoptosis was induced. Apoptosis staining confirmed the existence of apoptotic cells, and the typical characteristics of apoptotic karyopyknosis were observed.[54]

Thus, our analysis captures the complexity of the lethal effect of Iy on *A. aegypti* larvae. The peritrophic membrane is the first barrier of the midgut defense system, which can protect epithelial cells from mechanical damage, promote digestion, and facilitate the absorption of nutrients in the insects.[55,56] Furthermore, the microvilli provide an enlarged surface area for nutrient absorption.[57] When they are damaged, it will inevitably lead to poor nutrient absorption, insufficient energy supply, and damage to mitochondrial functions, which affect energy production. *A. aegypti* needs sufficient energy to complete its life cycle. When the nutrient intake is insufficient, along with reduced energy storage, it can lead to the death of *A. aegypti*.[58] Therefore, the larval stage continues to die, and even if it can enter the pupa stage, there are dead pupae and abnormal eclosion. Furthermore, some studies demonstrated that when the integrity of epithelial cells is destroyed, the proliferation and differentiation of epithelial cells in the process of development are affected, leading to the emergence of malformed adult mosquitoes.[59,60] Therefore, even at a sublethal concentration of Iy, it can have a negative effect on the growth, development, and metamorphosis of *A. aegypti*.

In conclusion, the mechanism of the lethal effect of Iy in *A. aegypti* larvae can be proposed. When the antioxidant system is out of balance, it causes oxidative damage to the midgut, leading to histopathological changes. ROS accumulates continuously, and apoptosis is induced, which leads to apoptosis of midgut cells, eventually to the death of the *A. aegypti* larva. However, although the control of *A. aegypti* at sublethal Iy concentrations appeared to be effective under laboratory conditions, the toxic effect of Iy on *A. aegypti* in a natural environment needs to be further studied. Hence, there is promising potential for the application of Iy in mosquito prevention and control.

AUTHOR INFORMATION

Corresponding Author

Yanping Luo − *Key Laboratory of Green Prevention and Control of Tropical Plant Diseases and Pests, Ministry of Education, College of Plant Protection, Hainan University, Haikou, Hainan 570228, P.R. China*; orcid.org/0000-0002-2184-4291; Phone: +86-13648634489; Email: yanpluo2012@hainanu.edu.cn

Authors

Jiecheng Wu − *Key Laboratory of Green Prevention and Control of Tropical Plant Diseases and Pests, Ministry of Education, College of Plant Protection, Hainan University, Haikou, Hainan 570228, P.R. China*

Lanying Wang − *Key Laboratory of Green Prevention and Control of Tropical Plant Diseases and Pests, Ministry of Education, College of Plant Protection, Hainan University, Haikou, Hainan 570228, P.R. China*

Yunfei Zhang − *Key Laboratory of Green Prevention and Control of Tropical Plant Diseases and Pests, Ministry of Education, College of Plant Protection, Hainan University, Haikou, Hainan 570228, P.R. China*

Shujing Zhang − *Key Laboratory of Green Prevention and Control of Tropical Plant Diseases and Pests, Ministry of Education, College of Plant Protection, Hainan University, Haikou, Hainan 570228, P.R. China*

Shakil Ahmad − *Key Laboratory of Green Prevention and Control of Tropical Plant Diseases and Pests, Ministry of Education, College of Plant Protection, Hainan University, Haikou, Hainan 570228, P.R. China*

Complete contact information is available at: https://pubs.acs.org/10.1021/acs.jafc.0c07237

Author Contributions

§J.W. and L.W. contributed equally to this work.

Notes

The authors declare no competing financial interest.

ACKNOWLEDGMENTS

This work was supported by the National Natural Science Foundation of China (31860513) and the Hainan Provincial Natural Science Foundation of China (2018CXTD335).

ABBREVIATIONS

Iy, 2-thiophenylfuranocoumarin; ROS, reactive oxygen species; ETC, electron transport chain; NADH, nicotinamide adenine dinucleotide; $FADH_2$, flavin adenine dinucleotide; TCA, tricarboxylic acid; SOD, superoxide dismutase; H_2O_2, hydrogen peroxide; CAT, catalase; GPx, glutathione peroxidase; GSH, glutathione; GR, glutathione reductase; GSSG, oxidized glutathione; MDA, malondialdehyde; AeIAP1, *Aedes aegypti*

inhibitor of apoptosis protein 1; MMP, mitochondrial membrane potential; TLC, thin-layer chromatography; NBS, *N*-bromosuccinimide; THF, tetrahydrofuran; $^1O_2$, singlet oxygen; ESR, electron spin resonance; DCFH-DA, 2,7-dichloro-hydrofluorescein diacetate; PBS, phosphate-buffered saline; TEM, transmission electron microscopy; CS, citric acid synthase; ICDHm, isocitrate dehydrogenase; α-KGDH, α-ketoglutarate dehydrogenase; JC-1, 5,5,6,6-tetrachloro-1,1,3,3-tetraethylbenzimidazolyl carbocyanine iodide; FITC, fluorescein isothiocyanate; TUNEL, transferase dUTP nick end labeling; RT-qPCR, quantitative reverse transcription PCR; RP7S, ribosomal protein 7S; PPh_3, triphenylphosphine; NMR, nuclear magnetic resonance; α-T, alpha-terthienyl; LC, lethal concentration; TDT, terminal deoxynucleotidyl transferase

REFERENCES

(1) Raquet, N.; Schrenk, D. Application of the equivalency factor concept to the phototoxicity and −genotoxicity of furocoumarin mixtures. *Food Chem. Toxicol.* **2014**, *68*, 257−266.

(2) Roselli, S.; Olry, A.; Vautrin, S.; Coriton, O.; Ritchie, D.; Galati, G.; Navrot, N.; Krieger, C.; Vialart, G.; Bergés, H.; Bourgaud, F.; Hehn, A. A bacterial artificial chromosome (BAC) genomic approach reveals partial clustering of the furanocoumarin pathway genes in parsnip. *Plant J.* **2017**, *89*, 1119−1132.

(3) Melough, M. M.; Lee, S. G.; Cho, E.; Kim, K.; Provatas, A. A.; Perkins, C.; Park, M. K.; Qureshi, A.; Chun, O. K. Identification and Quantitation of Furocoumarins in Popularly Consumed Foods in the U.S. Using QuEChERS Extraction Coupled with UPLC-MS/MS Analysis. *J. Agric. Food Chem.* **2017**, *65*, 5049−5055.

(4) Ahmed, S.; Khan, H.; Aschner, M.; Mirzae, H.; Küpeli Akkol, E.; Capasso, R. Anticancer Potential of Furanocoumarins: Mechanistic and Therapeutic Aspects. *Int. J. Mol. Sci.* **2020**, *21*, 5622.

(5) Pynam, H.; Dharmesh, S. M. Antioxidant and anti-inflammatory properties of marmelosin from Bael (*Aegle marmelos* L.); Inhibition of TNF-α mediated inflammatory/tumor markers. *Biomed. Pharmacother.* **2018**, *106*, 98−108.

(6) Stern, R. S.; PUVA Follow-up Study. The risk of squamous cell and basal cell cancer associated with psoralen and ultraviolet A therapy: A 30-year prospective study. *J. Am. Acad. Dermatol.* **2012**, *66*, 553−562.

(7) Melough, M. M.; Cho, E.; Chun, O. K. Furocoumarins: A review of biochemical activities, dietary sources and intake, and potential health risks. *Food Chem. Toxicol.* **2018**, *113*, 99−107.

(8) Carbone, A.; Montalbano, A.; Spanò, V.; Musante, I.; Galietta, L. J. V.; Barraja, P. Furocoumarins as multi-target agents in the treatment of cystic fibrosis. *Eur. J. Med. Chem.* **2019**, *180*, 283−290.

(9) Scott, B. R.; Pathak, M. A.; Mohn, G. R. Molecular and genetic basis of furocoumarin reactions. *Mutat. Res.* **1976**, *39*, 29−74.

(10) Ahmad, S. I.; Yokoi, M.; Hanaoka, F. Identification of new scavengers for hydroxyl radicals and superoxide dismutase by utilising ultraviolet A photoreaction of 8-methoxypsoralen and a variety of mutants of Escherichia coli: implications on certain diseases of DNA repair deficiency. *J. Photochem. Photobiol., B* **2012**, *116*, 30−36.

(11) Melough, M. M.; Chun, O. K. Dietary furocoumarins and skin cancer: A review of current biological evidence. *Food Chem. Toxicol.* **2018**, *122*, 163−171.

(12) Miolo, G.; Sturaro, G.; Cigolini, G.; Menilli, L.; Tasso, A.; Zago, I.; Conconi, M. T. 4,6,4′-trimethylangelicin shows high antiproliferative activity on DU145 cells under both UVA and blue light. *Cell Proliferation* **2018**, *51*, No. e12430.

(13) Martínez-Reyes, I.; Diebold, L. P.; Kong, H.; Schieber, M.; Huang, H.; Hensley, C. T.; Mehta, M. M.; Wang, T.; Santos, J. H.; Woychik, R.; Dufour, E.; Spelbrink, J. N.; Weinberg, S. E.; Zhao, Y.; DeBerardinis, R. J.; Chandel, N. S. TCA Cycle and Mitochondrial Membrane Potential Are Necessary for Diverse Biological Functions. *Mol. Cell* **2016**, *61*, 199−209.

(14) Willems, P. H. G. M.; Rossignol, R.; Dieteren, C. E. J.; Murphy, M. P.; Koopman, W. J. H. Redox homeostasis and mitochondrial dynamics. *Cell Metab.* **2015**, *22*, 207−218.

(15) Nolfi-Donegan, D.; Braganza, A.; Shiva, S. Mitochondrial Electron Transport Chain: Oxidative Phosphorylation, Mitochondrial Oxidant Production, and Methods of Measurement. *Redox. Biol.* **2020**, *37*, 101674.

(16) Angelova, P. R.; Abramov, A. Y. Functional role of mitochondrial reactive oxygen species in physiology. *Free Radical Biol. Med.* **2016**, *100*, 81−85.

(17) Zhuang, S.; Yu, R.; Zhong, J.; Liu, P.; Liu, Z. Rhein from Rheum rhabarbarum Inhibits Hydrogen-Peroxide-Induced Oxidative Stress in Intestinal Epithelial Cells Partly through PI3K/Akt-Mediated Nrf2/HO-1 Pathways. *J. Agric. Food Chem.* **2019**, *67*, 2519−2529.

(18) Hutnick, M. A.; Ahsanuddin, S.; Guan, L.; Lam, M.; Baron, E. D.; Pokorski, J. K. PEGylated Dendrimers as Drug Delivery Vehicles for the Photosensitizer Silicon Phthalocyanine Pc 4 for Candidal Infections. *Biomacromolecules* **2017**, *18*, 379−385.

(19) Shah, D.; Sah, S.; Nath, S. K. Interaction between glutathione and apoptosis in systemic lupus erythematosus. *Autoimmun Rev.* **2013**, *12*, 741−751.

(20) Nasimian, A.; Farzaneh, P.; Tamanoi, F.; Bathaie, S. Z. Cytosolic and mitochondrial ROS production resulted in apoptosis induction in breast cancer cells treated with Crocin: The role of FOXO3a, PTEN and AKT signaling. *Biochem. Pharmacol.* **2020**, *177*, 113999.

(21) Rossbach, L. M.; Oughton, D. H.; Maremonti, E.; Coutris, C.; Brede, D. A. In vivo assessment of silver nanoparticle induced reactive oxygen species reveals tissue specific effects on cellular redox status in the nematode *Caenorhabditis elegans*. *Sci. Total Environ.* **2020**, *721*, 137665.

(22) Jahedsani, A.; Khezri, S.; Ahangari, M.; Bakhshii, S.; Salimi, A. Apigenin attenuates Aluminum phosphide-induced cytotoxicity via reducing mitochondrial/Lysosomal damages and oxidative stress in rat Cardiomyocytes. *Pestic. Biochem. Physiol.* **2020**, *167*, 104585.

(23) Kuzmic, M.; Galas, S.; Lecomte-Pradines, C.; Dubois, C.; Dubourg, N.; Frelon, S. Interplay between ionizing radiation effects and aging in *C. elegans*. *Free Radical Biol. Med.* **2019**, *134*, 657−665.

(24) Batool, K.; Alam, I.; Jin, L.; Xu, J.; Wang, J.; Huang, E.; Guan, X.; Yu, X.-Q.; Zhang, L. CTLGA9 interacts with ALP1 and APN receptors to modulate Cry11Aa toxicity in *Aedes aegypti*. *J. Agric. Food Chem.* **2019**, *67*, 8896−8904.

(25) Tok, F.; Kocyigit-Kaymakcioglu, B.; Tabanca, N.; Estep, A. S.; Gross, A. D.; Geldenhuys, W. J.; Becnel, J. J.; Bloomquist, J. R. Synthesis and structure−activity relationships of carbohydrazides and 1, 3, 4-oxadiazole derivatives bearing an imidazolidine moiety against the yellow fever and dengue vector, Aedes aegypti. *Pest Manag. Sci.* **2018**, *74*, 413−421.

(26) Wan, Y.; Wu, S.; Zheng, S.; Liang, E.; Liu, S.; Yao, X.; Zhu, Q. A series of octahydroquinazoline-5-ones as novel inhibitors against dengue virus. *Eur. J. Med. Chem.* **2020**, *200*, 112318.

(27) Chang, K. P.; Kolli, B. K.; The New Light Group. New″ light″ for one-world approach toward safe and effective control of animal diseases and insect vectors from leishmaniac perspectives. *Parasites Vectors* **2016**, *9*, 396.

(28) Cooper, D. M.; Granville, D. J.; Lowenberger, C. The insect caspases. *Apoptosis.* **2009**, *14*, 247−256.

(29) Liu, Q.; Clem, R. J. Defining the core apoptosis pathway in the mosquito disease vector *Aedes aegypti*: the roles of iap1, ark, dronc, and effector caspases. *Apoptosis.* **2011**, *16*, 105−113.

(30) Wang, H.; Clem, R. J. The role of IAP antagonist proteins in the core apoptosis pathway of the mosquito disease vector *Aedes aegypti*. *Apoptosis.* **2011**, *16*, 235−248.

(31) Zhang, J.; Ahmad, S.; Wang, L. Y.; Han, Q.; Zhang, J. C.; Luo, Y. P. Cell death induced by α-terthienyl via reactive oxygen species-mediated mitochondrial dysfunction and oxidative stress in the midgut of *Aedes aegypti* larvae. *Free Radical Biol. Med.* **2019**, *137*, 87−98.

https://dx.doi.org/10.1021/acs.jafc.0c07237
J. Agric. Food Chem. 2021, 69, 1091−1106

(32) Timoshnikov, V. A.; Kobzeva, T. V.; Polyakov, N. E.; Kontoghiorghes, G. J. Inhibition of Fe(2+)- and Fe(3+)- induced hydroxyl radical production by the iron-chelating drug deferiprone. *Free Radical Biol. Med.* **2015**, *78*, 118−122.
(33) Xia, Q.; Wei, L.; Zhang, Y.; Kong, H.; Shi, Y.; Wang, X.; Chen, X.; Han, L.; Liu, K. Psoralen Induces Developmental Toxicity in Zebrafish Embryos/Larvae Through Oxidative Stress, Apoptosis, and Energy Metabolism Disorder. *Front. Pharmacol.* **2018**, *9*, 1457.
(34) Vaidyanathan, R.; Scott, T. W. Apoptosis in mosquito midgut epithelia associated with West Nile virus infection. *Apoptosis.* **2006**, *11*, 1643−1651.
(35) Dubey, S. K.; Shrinet, J.; Sunil, S. *Aedes aegypti* microRNA, miR-2944b-5p interacts with 3'UTR of chikungunya virus and cellular target vps-13 to regulate viral replication. *PLoS Negl Trop Dis.* **2019**, *13*, No. e0007429.
(36) Ganesan, P.; Stalin, A.; Paulraj, M. G.; Balakrishna, K.; Ignacimuthu, S.; Al-Dhabi, N. A. Biocontrol and non-target effect of fractions and compound isolated from Streptomyces rimosus on the immature stages of filarial vector *Culex quinquefasciatus Say* (Diptera: Culicidae) and the compound interaction with Acetylcholinesterase (AChE1). *Ecotoxicol. Environ. Saf.* **2018**, *161*, 120−128.
(37) Edwards, M. J.; Jacobs-Lorena, M. Permeability and disruption of the peritrophic matrix and caecal membrane from *Aedes aegypti* and *Anopheles gambiae* mosquito larvae. *J. Insect Physiol.* **2000**, *46*, 1313−1320.
(38) Zhang, J.; Zhu, K. Y. Characterization of a chitin synthase cDNA and its increased mRNA level associated with decreased chitin synthesis in Anopheles quadrimaculatus exposed to diflubenzuron. *Insect Biochem. Mol. Biol.* **2006**, *36*, 712−725.
(39) Eng, M. W.; Van Zuylen, M. N.; Severson, D. W. Apoptosis-related genes control autophagy and influence DENV-2 infection in the mosquito vector, *Aedes aegypti*. *Insect Biochem. Mol. Biol.* **2016**, *76*, 70−83.
(40) Dichiara, M.; Prezzavento, O.; Marrazzo, A.; Pittalà, V.; Salerno, L.; Rescifina, A.; Amata, E. Recent advances in drug discovery of phototherapeutic non-porphyrinic anticancer agents. *Eur. J. Med. Chem.* **2017**, *142*, 459−485.
(41) Zamani, E.; Shaki, F.; Abediankenari, S.; Shokrzadeh, M. Acrylamide induces immunotoxicity through reactive oxygen species production and caspase-dependent apoptosis in mice splenocytes via the mitochondria-dependent signaling pathways. *Biomed. Pharmacother.* **2017**, *94*, 523−530.
(42) Fernandes, K. M.; Tomé, H. V. V.; Miranda, F. R.; Conçalves, W. G.; Pascini, T. V.; Serrão, J. E.; Martins, G. F. *Aedes aegypti* larvae treated with spinosad produce adults with damaged midgut and reduced fecundity. *Chemosphere* **2019**, *221*, 464−470.
(43) Kelkenberg, M.; Odman-Naresh, J.; Muthukrishnan, S.; Merzendorfer, H. Chitin is a necessary component to maintain the barrier function of the peritrophic matrix in the insect midgut. *Insect Biochem. Mol. Biol.* **2015**, *56*, 21−28.
(44) Chowdhury, A. R.; Zielonka, J.; Kalyanaraman, B.; Hartley, R. C.; Murphy, M. P.; Avadhani, N. G. Mitochondria-Targeted Paraquat and Metformin Mediate ROS Production to Induce Multiple Pathways of Retrograde Signaling: A dose-dependent phenomenon. *Redox. Biol.* **2020**, *36*, 101606.
(45) Markevich, N. I.; Galimova, M. H.; Markevich, L. N. Hysteresis and bistability in the succinate-CoQ reductase activity and reactive oxygen species production in the mitochondrial respiratory Complex II. *Redox Biol.* **2020**, 101630.
(46) Zorov, D. B.; Juhaszova, M.; Sollott, S. J. Mitochondrial reactive oxygen species (ROS) and ROS-induced ROS release. *Physiol. Rev.* **2014**, *94*, 909−950.
(47) Meng, D.; Zhang, P.; Zhang, L.; Wang, H.; Ho, C. T.; Li, S.; Shahidi, F.; Zhao, H. Detection of cellular redox reactions and antioxidant activity assays. *J. Funct. Foods.* **2017**, *37*, 467−479.
(48) Quijano, C.; Trujillo, M.; Castro, L.; Trostchansky, A. Interplay between oxidant species and energy metabolism. *Redox. Biol.* **2016**, *8*, 28−42.
(49) Bian, M.; Fan, R.; Jiang, G.; Wang, Y.; Lu, Y.; Liu, W. Halo and Pseudohalo Gold(I)−NHC Complexes Derived from 4,5-Diarylimidazoles with ExcellentIn VitroandIn VivoAnticancer Activities Against HCC. *J. Med. Chem.* **2020**, *63*, 9197−9211.
(50) Marie, M.; Bigot, K.; Angebault, C.; Barrau, C.; Gondouin, P.; Pagan, D.; Fouquet, S.; Villette, T.; Sahel, J.-A.; Lenaers, G.; Picaud, S. Light action spectrum on oxidative stress and mitochondrial damage in A2E-loaded retinal pigment epithelium cells. *Cell Death Dis.* **2018**, *9*, 287.
(51) Xiao, J.; Wu, C.; He, Y.; Guo, M.; Peng, Z.; Liu, Y.; Liu, L.; Dong, L.; Guo, Z.; Zhang, R.; Zhang, M. Rice Bran Phenolic Extract Confers Protective Effects against Alcoholic Liver Disease in Mice by Alleviating Mitochondrial Dysfunction via the PGC-1α-TFAM Pathway Mediated by microRNA-494-3p. *J. Agric. Food Chem.* **2020**, *68*, 12284−12294.
(52) Napolitano, G.; Fasciolo, G.; Di Meo, S.; Venditti, P. Vitamin E Supplementation and Mitochondria in Experimental and Functional Hyperthyroidism: A Mini-Review. *Nutrients* **2019**, *11*, 2900.
(53) Liu, S.-Y.; Song, J.-Y.; Fan, B.; Pan, Y.-R.; Che, L.; Sun, Y.-J.; Li, G.-Y. Resveratrol protects photoreceptors by blocking caspase- and PARP-dependent cell death pathways. *Free Radical Biol. Med.* **2018**, *129*, 569−581.
(54) Chen, G.; Zhang, P.; Huang, T.; Yu, W.; Lin, J.; Li, P.; Chen, K. Polysaccharides from Rhizopus nigricans mycelia induced apoptosis and G2/M arrest in BGC-823 cells. *Carbohydr. Polym.* **2013**, *97*, 800−808.
(55) Liu, X.; Cooper, A. M. W.; Zhang, J.; Zhu, K. Y. Biosynthesis, modifications and degradation of chitin in the formation and turnover of peritrophic matrix in insects. *J. Insect Physiol.* **2019**, *114*, 109−115.
(56) Toprak, U.; Erlandson, M.; Baldwin, D.; Karcz, S.; Wan, L.; Coutu, C.; Gillott, C.; Hegedus, D. D. Identification of the *Mamestra configurata* (Lepidoptera: Noctuidae) peritrophic matrix proteins and enzymes involved in peritrophic matrix chitin metabolism. *Insect Sci.* **2016**, *23*, 656−674.
(57) Li, H.; Zhang, J.; Ma, T.; Li, C.; Ma, Z.; Zhang, X. Acting target of toosendanin locates in the midgut epithelium cells of *Mythimna separate* Walker larvae (lepidoptera: Noctuidae). *Ecotoxicol. Environ. Saf.* **2020**, *201*, 110828.
(58) Sasmita, H. I.; Tu, W.-C.; Bong, L.-J.; Neoh, K.-B. Effects of larval diets and temperature regimes on life history traits, energy reserves and temperature tolerance of male *Aedes aegypti* (Diptera: Culicidae): optimizing rearing techniques for the sterile insect programmes. *Parasites. Vectors.* **2019**, *12*, 578.
(59) Bibi, R.; Tariq, R. M.; Rasheed, M. Toxic assessment, growth disrupting and neurotoxic effects of red seaweeds' botanicals against the dengue vector mosquito *Aedes aegypti* L. *Ecotoxicol. Environ. Saf.* **2020**, *195*, 110451.
(60) de Santa Silva, L. L.; Fernandes, K. M.; Miranda, F. R.; Silva, S. C. C.; Coelho, L. C. B. B.; do Amaral Ferraz Navarro, D. M.; Napoleão, T. H.; Martins, G. F.; Paiva, P. M. G. Exposure of mosquito (*Aedes aegypti*) larvae to the water extract and lectin- rich fraction of Moringa oleifera seeds impairs their development and future fecundity. *Ecotoxicol. Environ. Saf.* **2019**, *183*, 109583.

https://dx.doi.org/10.1021/acs.jafc.0c07237
J. Agric. Food Chem. 2021, 69, 1091−1106